Using Infrared Thermography to Image the Drying of Polymer Surfaces

A Thesis
Presented to
The Academic Faculty

by

Gregory M. Fike

In Partial Fulfillment
Of the Requirements for the Degree
Master of Science in Chemical Engineering

School of Chemical and Biomolecular Engineering
Georgia Institute of Technology
August 2004

Using Infrared Thermography to Image the Drying of Polymer Surfaces

Approved by:

Dr. Sujit Banerjee, Advisor

Dr. Yulin Deng

Dr. Timothy Patterson

Date Approved: August 30, 2004

To my wife, Melissa.

ACKNOWLEDGMENT

Grateful acknowledgment is made for the valuable suggestions and guidance of my advisor, Sujit Banerjee and also to the members of my committee, Yulin Deng and Timothy Patterson.

The financial support of the Institute of Paper Science and Technology and its member companies is also greatly appreciated.

TABLE OF CONTENTS

LIST OF FIGURES

LIST OF SYMBOLS AND ABBREVIATIONS

AFM	Atomic Force Microscope
c	Speed of light
CD	Cross Direction
cm	Centimeter
COV	Coefficient of Variance
ΔT	Temperature difference
ε	Emissivity
E	Exponential (10^)
FIR	Far Infrared
h	Planck's constant
I	Current
IR	Infrared
k	Boltzmann's constant
K	Kelvin
kHz	Kilohertz
λ	Wavelength
λ_{max}	Maximum wavelength
m	meter
MC	Moisture Content
MIR	Mid Infrared
mm	Millimeter
μm	Micrometer
N	Newton

N_b	Number of photons emitted
NIR	Near Infrared
$N_{\lambda b}$	Number of photons emitted at wavelength λ
nm	Nanometer
^oC	Degrees Celsius
P	Power
π	pi = 3.141
PSA	Pressure Sensitive Adhesive
R	Resistance
RMS	Root Mean Square
σ	Stefan-Boltzmann constant
s	Second
T	Temperature
T_a	Absolute temperature
TRIR	Time Resolved Infrared Radiometry
W_b	Total radiant emittance
$W_{\lambda b}$	Emission of a blackbody at wavelength λ
$W_{\lambda o}$	Emission of an object at wavelength λ
w_{od}	Oven dry weight
w_w	Wet weight

SUMMARY

During the drying of a surface, the liquid evaporation acts to keep the temperature relatively constant, due to evaporative cooling. As the drying nears completion the liquid film begins to break, exposing areas that are no longer cooled through evaporation, which begin to heat. Although this heating can be measured with an Infrared (IR) camera, the sensitivity is often not sufficient to recognize the point at which the film breaks. Complicating the measurement is the changing emissivity that commonly occurs as objects dry.

The sensitivity and emissivity issues can be addressed by analyzing the temperature in the area of interest and computing the coefficient of variance (COV) of the temperature. This technique is compared to temperature and standard deviation measurements made with an IR camera and the COV technique is shown to be superior for determining when the liquid film breaks. The film breakage point is found to vary with temperature and material roughness in two industrially significant applications: the drying of wood flakes and the drying of polymer films.

Film breakage in wood flakes is related to detrimental finished quality problems and also to emission problems. The rate at which an adhesive dries affects the roughness of the polymer film and subsequently, the bond strength. The COV technique is used to predict the roughness of the finished polymer film. Use of the COV technique allows the drying of a liquid film to be visualized in a way that has been previously unreported.

1 INTRODUCTION

The manner in which a solvent evaporates from a surface can control the properties of the dried surface. For instance, when wood flakes are dried for the manufacture of oriented strand board, the evenness of drying impacts the surface properties of the flakes and can affect the strength of the adhesive bond when the flakes are subsequently glued together[1]. In another example, when a film is deposited from a solvent, the uniformity and topology of the film can be influenced by the rate of evaporation. These properties are important in many applications[2-6], and topology is often measured after deposition with techniques such as Atomic Force Microscopy (AFM)[3, 7, 8], Scanning Force Microscopy[9], Transmission Electron Microscopy[7], and optical microscopy[7, 8, 10]. Less common are techniques such as laser interferometry, shadowgraphy, and optical microscopy, where the film is monitored while it forms[10, 11].

IR thermography has been used as a tool in a number of applications in heat transfer[12-14], fluid dynamics[15], and corrosion[16]. In principle, IR thermography can detect the point at which surface dryout begins, because evaporative cooling is lost at this point and the surface temperature rises. However, the temperature rise is initially quite small and can be difficult to detect. The COV of the temperature (defined as the standard deviation of temperature divided by the average temperature) can detect the onset of surface dryout with greater sensitivity. The surface is now exposed in spots, which increases the temperature variations across the surface. The COV reflects these variations and is,

therefore, a much more sensitive measure of the early stages of liquid film breakage than is the average surface temperature.

Commonly, results from IR studies are presented as ΔT or RMS temperature, which is acceptable when measuring a homogenous sample[17, 18]. By dividing two temperature terms, changes in the emissivity of the surface during drying are reduced. This is beneficial in cases where the emissivity of the material is either unknown or where it changes, e.g. due to the evaporation of water or to oxidation of the surface during measurement[19].

In this thesis the technique is demonstrated with two applications: wood drying where the surface is rough, and also the deposition of an organic film from water on a smooth metal surface. The COV of the surface temperature accurately identifies the point at which the surface begins to dry out or when the surface film breaks.

2 LITERATURE REVIEW

The literature review presented here serves several purposes including introducing the fundamental concepts of IR thermography. Also presented are applications of IR thermography relevant to the paper industry and the study of film drying.

IR thermography is used to determine the temperature of an object by measuring the vibrations produced by any material at temperatures above absolute zero. This technology is currently used in a number of applications ranging from the defense industry to semiconductor processing. IR thermography is capable of detecting small changes in temperature with very good resolution without contacting the measured object, which allows variations in composition to be determined in a nondestructive manner. Measurements of this type are not possible with typical thermometers or thermocouples. This thesis will begin by discussing the fundamental principles that allow IR thermography to be effective and will continue to discuss some of the common applications where the technology is used. Additionally, the thesis will present the applications specific to the paper industry.

The main advantage of IR thermography is that it is a noncontact measurement and is considered the "most versatile of the nondestructive testing (NDT) techniques[20]." These types of techniques can be very helpful when dealing with a number of situations such as measuring a moving, fragile, small, or hazardous target. This NDT is also useful when multiple measurements are needed from a remote target[21]. The result of the

thermal mapping of a surface is typically called a thermogram. IR thermography is possible because of the discovery of radiation beyond the visible spectrum around the year 1800 by William Herchel[21]. Since then, many advances have been made to bring the technology to its present point.

2.1 IR Thermography Theory

All objects above absolute zero (-273.15 ^{o}C or 0 K) emit radiation. Some of this radiation falls in the IR spectrum, which is radiation that has larger wavelengths and lower energies than that in the visible spectrum. The IR spectrum begins at 0.75 μm and continues to 1000 μm. The upper and lower limits of the spectrum are arbitrary, especially the cutoffs between the subcategories (near, mid, and far)[22]. Figure 2.1 presents a visual representation of the entire electromagnetic spectrum with the IR spectrum highlighted.

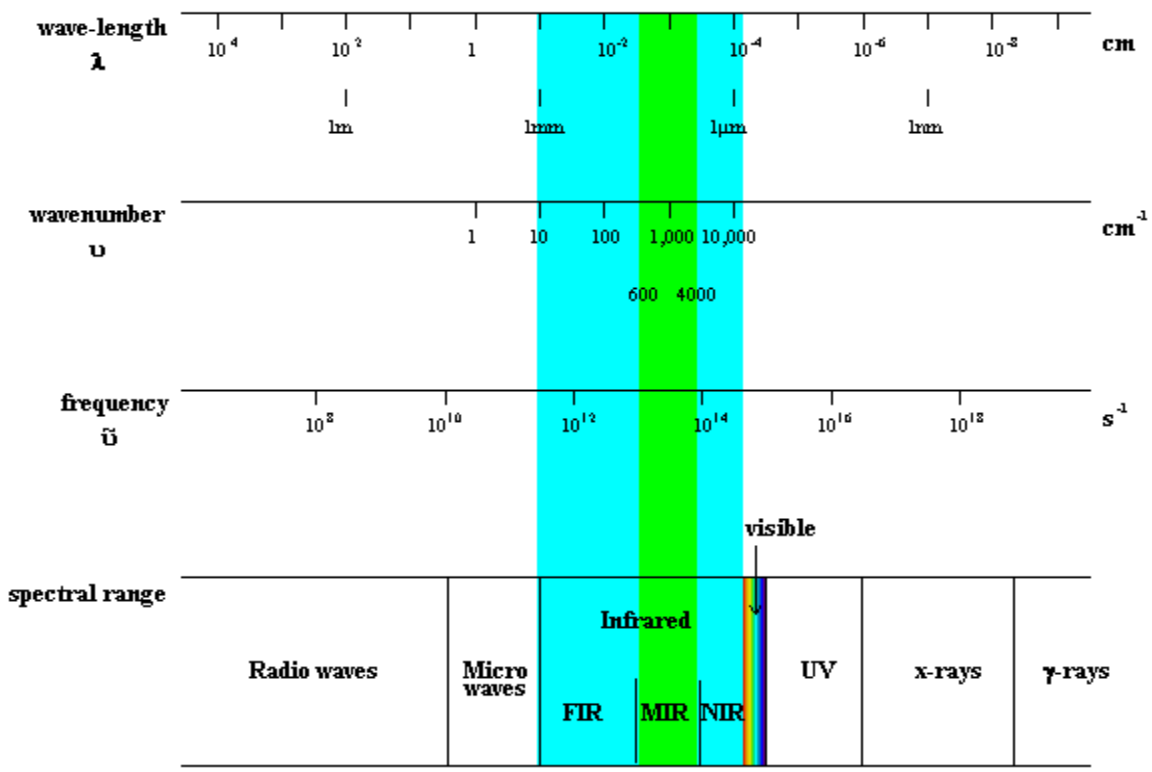

Figure 2.1: Typical description of the electromagnetic spectrum[23].

In order to describe objects and how they emit energy, it is first useful to discuss the concept of a blackbody. Although the idea of a blackbody is ideal in nature, it allows discussions about radiation to focus on the physics of the process rather than the corrections needed to apply the concepts to a wide range of objects. The blackbody object absorbs all of the radiation that contacts it regardless of the wavelength of the radiation. The opposite of a blackbody is a perfect mirror, an object that reflects all of the radiation to which it is subjected. Between these two extremes is a graybody. At a particular wavelength, the object will emit a percentage of what a blackbody would emit. This

difference is corrected with a material property known as emissivity, which will be discussed later in the theory section.

Once the energy is absorbed it is emitted to the environment as explained by Kirchhoff's law, which states that at equilibrium the radiation that is emitted must be equal to the radiation that is absorbed[19, 24].

Planck's equation describes the amount of energy emitted over an area at a particular wavelength (Equation 2.1). The wavelength where the maximum energy is emitted is found by differentiating Planck's equation. The Stefan-Boltzmann equation relates the total power emitted by an object to the absolute temperature. This equation is found by integrating Planck's equation over the wavelengths of interest. IR thermography measures the energy emitted and uses the relationship in the Stefan-Boltzmann equation to determine the temperature of the object. The Stefan-Boltzmann equation is modified with the emissivity of the object to correct for the fact that the objects do not act as blackbodies. Equation 2.8, presented later, shows the relationship as it is used in IR thermography.

The remainder of the theory section presents the equations of interest to IR thermography as well as graphical representations to show the trends in the emission of power that dictate the measurement of temperature by IR thermography. The theory begins with the energy emitted that is described by Planck's equation.

$$W_{\lambda o} = \frac{2\pi hc^2}{\lambda^5 * \left(e^{hc/\lambda k T_a} - 1 \right)} [=] Watts / m^2 * m$$

Equation 2.1

Where,

$W_{\lambda o}$ = emittance at wavelength λ

c = speed of light = $3E^8$ m/s

h = Planck's constant = $6.6E^{-34}$ J/s

k = Boltzmann's constant = $1.4E^{-23}$ J/K

T_a = Absolute Temperature (K)

λ = Wavelength (m)

Planck's equation is often written with the units of wavelength as μm rather than m. This is done by multiplying the above expression by 1 E^{-6}.

Planck's equation can be solved at any temperature for the emittance that corresponds to a particular wavelength of radiation. An example of this is shown in Figure 2.2. It is important to note that as temperature increases, the magnitude of the peak emittance becomes significantly larger and the peak occurs at lower wavelengths.

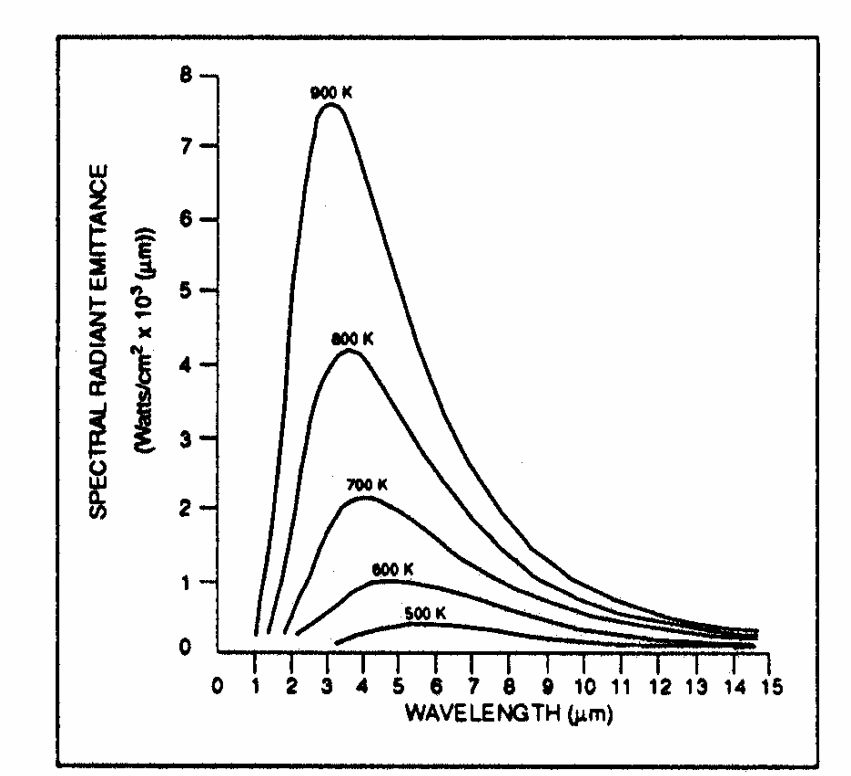

Figure 2.2: Planck's equation solved for various temperatures[19].

The maximum emittance described by Planck's equation is found by simply differentiating Planck's equation with respect to λ. By inserting the appropriate constants into the equation, the expression for the wavelength where the maximum emittance occurs is expressed by the following, which is known as Wien's Displacement Law:

$$\lambda_{max} = \frac{2898}{T}[=]\ \mu m \qquad \textbf{Equation 2.2}$$

This expression shows the inverse temperature relationship that governs the wavelength where the maximum emittance occurs. Figure 2.3 shows the emittance versus wavelength

curves with a dotted line that represents Wien's Displacement Law. For the emission to be visible, the temperature must be at least 700 K—this is indicated by Wien's law and Planck's equation[25].

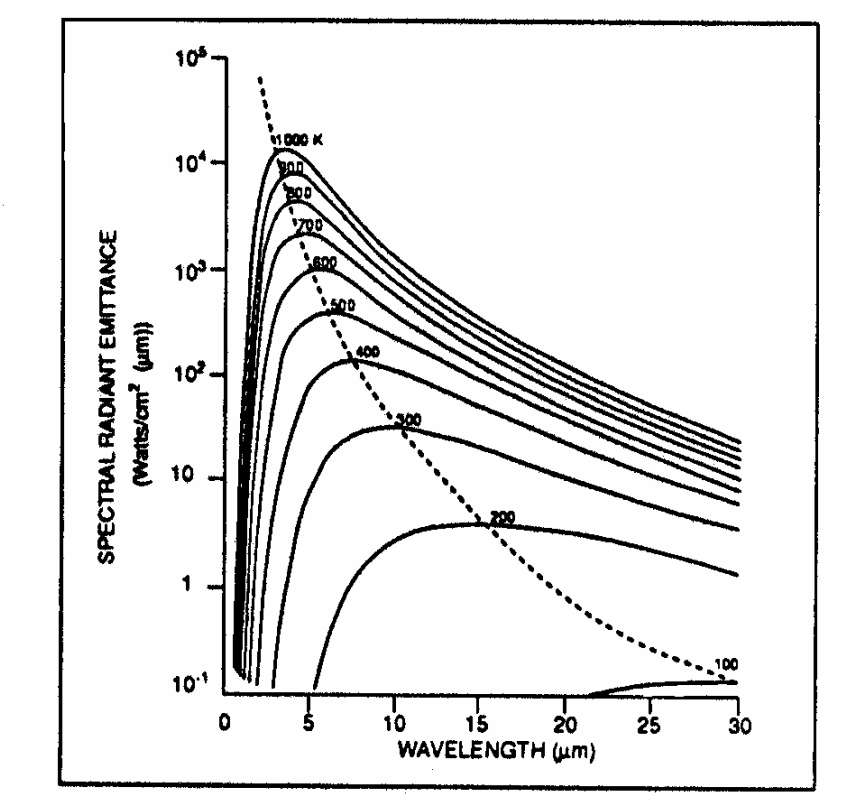

Figure 2.3: Blackbody emission with Wien's Displacement law[19].

Finally, the total emissive power of a radiating blackbody can be found by integrating Planck's equation over a range of wavelengths. The graphical representation of the expression is the area under the Planck's equation curve, also known as the Stefan-Boltzmann Law, and is given in Equation 2.3.

$$W_b = \sigma T_a^{\,4} [=] \frac{Watts}{m^2}$$ **Equation 2.3**

Where,

W_b = Total Radient Emittance

σ = Stefan-Boltzmann constant = 5.67 E^{-8} $W*m^{-2}*K^{-4}$

The Stefan-Boltzmann equation is used to relate the emittance of a blackbody to the absolute temperature of the object. Because a measured energy emission can be converted to temperature, the concept of remote temperature measurement such as IR thermography becomes reasonable.

Although the previously mentioned equations deal with the energy emitted by a radiating body, the energy is not emitted continuously. The energy is emitted as photons, which are small bursts of energy. The energy associated with a single photon varies only with wavelength and is given by hc/λ. Therefore, each of the above expressions can be altered to account for the number of photons released by dividing by the energy of a photon. A photon detector uses semiconductor technology to determine the number of photons from the amount of energy collected by the detector[26]. The number of photons emitted ($N_{\lambda b}$) is given by Planck's equation divided by the photon's energy.

$$N_{\lambda b} = \frac{2\pi c}{\lambda^4\left(e^{hc/\lambda kT} - 1\right)} * E^{-6} [=] \frac{photons}{s * m^2 * \mu m}$$ **Equation 2.4**

Similarly, Wien's displacement law gives the wavelength where the maximum photon emission occurs as the following:

$$\lambda_{max} = \frac{3663}{T_a} [=] \mu m$$ **Equation 2.5**

Finally, the Stefan-Boltzmann formula relates the number of photons emitted to the temperature of the measured object. This relationship is commonly used by thermography techniques that utilize photon counters as the measurement device.

$$N_b = \frac{0.37\sigma T_a^{\ 3}}{k} [=] \frac{photons}{s * m^2}$$ **Equation 2.6**

Each of the expressions presented have been developed for the specific case of perfect blackbody emission. Most objects do not operate as perfect blackbodies over the entire electromagnetic spectrum, but instead the emission is altered by any or all of the following three factors: light may be absorbed, reflected, or transmitted. When an object falls between a blackbody and a perfect reflector, it is known as a graybody. For most objects, the deviation from a blackbody is wavelength dependent, meaning that an object may act as a blackbody, graybody, and perfect reflector at different wavelengths. White paint, for example is white in the visible, gray around 2 μm, and it becomes black past 3 μm.

To mathematically account for the differences created by the deviations from blackbody radiation, the material property of emissivity (ε) is used. The emissivity is the ratio of the emission of an object ($W_{\lambda o}$) to that of a blackbody ($W_{\lambda b}$) at a particular wavelength and is mathematically represented as follows:

$$\varepsilon = \frac{W_{\lambda o}}{W_{\lambda b}} \qquad \textbf{Equation 2.7}$$

The emissivity ranges in value from 1 for a true blackbody to 0 for a perfect mirror. By knowing the emissivity at the wavelengths that are measured, the Stefan-Boltzmann equation can be adjusted to accurately calculate the temperature from the measured emittance. The property is purely experimental with no theoretical basis, requiring the values to be measured[27]. Additionally, changes due to temperature and geometry will alter the emissivity values of materials. It is also important to note that emissivity values are reported in several different forms. Spectral data is a function of wavelength and is commonly used for temperature measurements. Total emissivity is measured at a specific temperature and is typical of heat transfer data. Monochromatic data is specified for a very narrow range of wavelengths[28].

The following is the Stephen-Boltzmann equation adjusted for emissivity and is in the form that is useful for IR thermography and allows practical application of the theory:

$$W_b = \varepsilon \sigma T_a^{\,4} [=] \frac{Watts}{m^2}$$ **Equation 2.8**

Input of the emissivity is required to operate an IR camera and emissivity tables of common materials at specific wavelengths are readily available. Therefore, by knowing the emissivity, an IR camera is capable of calculating the temperature of an object by measuring the levels of radiation at a particular wavelength emitted by the object. Most surface temperature sensing systems utilize the mid-IR region (3000-5000 nm) for the measurement[29, 30].

2.2 Applications of IR Thermography

There are many applications where IR thermography is used throughout the world and in many different industries. Each application uses the theory in much the same way to accurately measure the temperature of objects in a non-invasive manner. Many of the uses are general in nature and deal with infrastructure and preventative maintenance. Most of these applications are useful in the paper industry simply because the industry uses mechanical and electrical equipment that is subject to every-day wear and tear.

Thermal sensing is most widely used in the monitoring of industrial plant operation, most commonly in preventative maintenance[21]. Thermal sensing is very effective in finding electrical problems before they become debilitating to a process. If part of a circuit has higher resistance than the rest of the circuit, it will have to dissipate the extra energy it obtains via Ohm's law ($P=I^2R$) by heating up. This temperature change could indicate a

worn connection or a poor contact. The high temperature would eventually lead to equipment failure. Short circuits in power supplies and motors are also detectable by the same method.

Electrical currents generated in ferrous metals by magnetic fields tend to heat the metal object. Induced currents are often the cause of temperature differences that arise in places where they are not expected. An interesting application of this induction heating is found in construction, where concrete walls that are reinforced with steel bars must be cut. The location of the bars can be found by applying a magnetic field to the wall and using thermal imaging to pinpoint the bars. This can ease construction and greatly reduce equipment wear. The use of thermal imaging to quickly determine the areas of a building that are prone to heat loss is another use that could ultimately lead to reducing costs associated with operating a structure. In general, temperature differences greater that 0.5 ^{o}C could point to potential problems and the area should be monitored closely. Also, when the thermal gradient between the hot spot and the surrounding areas or similar equipment is greater than 5 ^{o}C, the equipment should be repaired at the first opportunity[21].

Many mechanical systems can be monitored using thermal imaging. Elevated temperatures that arise from friction can be easily recognized with an IR camera. Bearings can be checked for deterioration and correct lubrication. Also, the correct alignment of drive shafts can be determined with thermal imaging. Steam traps are another piece of equipment that can benefit from the use of an IR camera. The purpose of

the steam trap is to remove condensate from a steam line. When operating properly, the area after the valve should be cooler than the rest of the line. When the valve sticks open, there will be no temperature difference. This can greatly reduce the amount of steam lost in a system.

Material testing is another area where thermal imaging is becoming more popular. Most applications involve supplying heat to the tested object, and measuring the thermal reaction of the object. The heat injection can occur as a constant, or it can be pulsed. Using a pulsed heat source is also known as time resolved infrared radiometry (TRIR) and is useful for gaining z-directional information about the location of a defect. These techniques have been used to detect inclusions or void spaces in welds, composite materials, and boiler tubes, among others.

Several applications of thermal imaging are more obvious to the general public. Many search and rescue missions utilize thermal imaging to locate lost people in darkness. The automotive industry has begun to install IR sensing systems in automobiles. These systems are capable of detecting radiation from another car or an animal at greater distances than the headlights can shine. The new systems are being marketed as night vision.

Thus far, only spot check applications of thermal imaging have been discussed. This technology is also used as a continuous process control element. One example of this is in the controlled cooling process of wire drawing. If the cooling is done to fast, it could

allow void spaces to develop in the wire, reducing strength and conductivity. If the wire is cooled too slowly, it reduces production, making temperature control essential. Glass making is another area where consistent cooling is necessary to ensure minimal deviations in the final product.

2.3 Paper Industry Applications

The use of thermal imaging increased in the paper industry in the last 10-15 years, and the number of applications has been growing as creative uses of the technology are introduced to the industry. Most of the general maintenance discussed with respect to electrical, mechanical, and infrastructure are also applicable in the paper industry. Specific processes in the industry allow for unique applications of the technology to be used. The specific uses will be discussed and compared to the conventional methods that thermal imaging has been used to eliminate.

IR thermography has been used in a wide range of ways throughout the paper industry, from the monitoring of the refractory lining of lime kilns to the identification of slower growing seedlings[31, 32]. The tremendous use of steam in the industry makes preventative maintenance of steam traps a valuable use of thermography[20, 31].

Perhaps the most interesting uses of IR thermography involve monitoring and troubleshooting of product quality problems such as uneven moisture profiles, coating streaks, and drying problems. The large differences in heat capacity between water and

paper-making solids (fiber and fillers) allow thermography to easily detect differences of moisture levels that exist in the paper web as it is being formed until it is on the reel. Paper with higher moisture content has a lower temperature than paper with lower moisture content.

The cross direction (CD) moisture profile of a sheet can be measured in several ways. The sheet can be measured directly in the press section by gathering an image of the sheet leaving a nip, or the wet felt can be measured if it is more convenient[33, 34]. The moisture profile of the wet felt can be measured before and after the Uhle boxes that are used to remove water from the felt. The CD efficiency of the Uhle boxes can be determined this way. Currently, a method exists using a microwave detection device that quantifies the water in the felts. Using IR thermography could improve safety levels during the measurement because unlike the microwave device, which requires the instrument to contact the felt and often places the operator in dangerous positions such as leaning over the operating paper machine, IR thermography could be done remotely. Using IR thermography could also increase the flexibility of the measurement by allowing the felts to be measured at the optimum position, rather than the conveniently reached position. IR thermography could also measure the felt before and after the Uhle boxes because it can be used from a distance, and many press sections are not accessible to a person with a piece of equipment.

Thermographs of the dryer cans also provide very important information regarding the operation of the dryer section of the paper machine. It has been reported that the

thermograph is capable of detecting low patterns across the surface of the dryer as small as 0.0015 inches[35]. This allows the loading of the doctor blades to be monitored in real time. The images also can be used to determine the effectiveness of the condensate removal systems as well as measuring the scaling of the metal inside of the dryer can. Uneven dryer temperatures, press loads, or Uhle box vacuum pressure lead to inconsistent CD moisture profiles. This then leads to roll building problems and to inefficiencies in drying. The drying problems arise because the papermaker is forced to overdry the sheet to eliminate wet streaks, thereby decreasing the efficiency of the process[36].

Another application where IR thermography is effective is in the real time analysis of roll covering defects. The method is used because it enables remote measurement of the moving rolls. It is reported that the technology is capable of detecting areas where protective roll coatings have been scraped off or are beginning to blister[37].

IR thermography has been used to aid in the identification of polymeric contaminants in recycled fiber, known as stickies. Taking advantage of the differing thermal conductivities, the polymers can be identified based on the relative cooling that each achieves following a period of heating[38]. This method showed promising results for pure stickies, but mill stickies are nearly always a mixture of several adhesives, reducing the accuracy of the method.

The operations associated with corrugating to make boxes require the medium to be heated to increase the flexibility prior to fluting[39]. The use of IR thermography could improve the operation by reducing the overheating and subsequent overuse of steam that would occur if the temperature is not monitored.

Another type of laboratory test that uses IR thermography is monitoring fiber temperature as it is placed under stress. This gives the observer additional information about the load-carrying abilities of the fibers and helps to determine the original location of the deformation in the fiber[40]. Common product quality issues such as cockle and curl are able to be quantified using IR thermography with controlled heating and cooling on a flat surface. The heating and cooling is monitored with IR thermography and the areas where the paper is not touching the surface because of cockle or curl is easily quantified with the technology[41].

These examples account for a few of the many uses for IR thermography in the paper industry. It is conceivable that formation studies can be performed starting at the slice and continuing to the reel, all with thermography. Areas in the paper that have higher basis weight due to more fiber being present would have a higher temperature due to the differences in specific heat between water and fiber (the specific heat of water is nearly three times that of fiber) and also due to differences in emissivity[41]. There are a number of areas where IR thermography could be used as an effective research tool.

2.4 Imaging of Water Evaporation

IR thermography has been used to image evaporating water with the primary purpose of understanding ocean movements. During evaporation, non-uniform cooling at the surface leads to instability in the liquid and subsequent flow. Flow derived from the effects of evaporation is called natural convection[42]. Saylor et al. have presented images, gathered with an IR camera functioning between 2 and 5 μm, which define the convection cells that develop during evaporation. They have also deposited a monolayer of surfactant on the water films to show the dampening effects of the surfactant on the surface driven flow. The results have also been coupled with a two component laser Doppler velocimeter system to confirm the presence of flow beneath the liquid surface[43, 44].

Figure 2.4 shows the results found by imaging both clean and surfactant covered water surfaces at two heat fluxes. The images represent approximately 15 cm square sections of water in a 15 cm deep tank. The high heat flux-clean water case in (a) shows significant temperature differences at the water surface. Adding a surfactant monolayer (b) reduces the small scale temperature perturbations while the large scale differences remain. At lower heat fluxes, there is less temperature difference for the clean system (c) and the addition of surfactant again reduces the small scale differences (d).

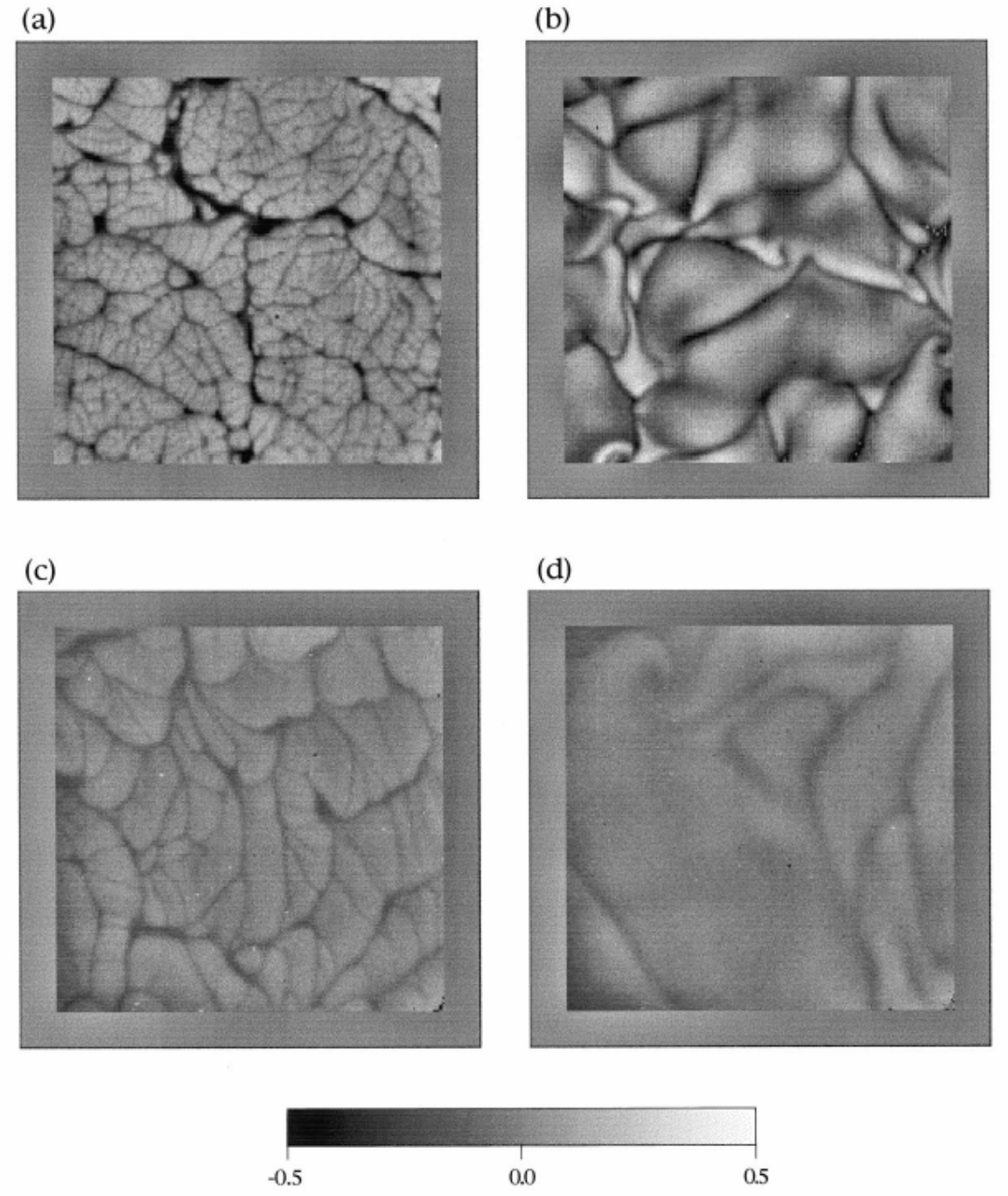

Figure 2.4: Temperature fields measured with IR thermography for evaporating water at various conditions. (a) High heat flux. (b) High heat flux with surfactant. (c) Low heat flux. (d) Low heat flux with surfactant[42]. The temperature scale indicates deviation from the average in ^{o}C.

The same group also presented the data shown in Figure 2.5[18]. This depiction better illustrates the progression as the heat flux increases. The RMS of the temperature was also shown to increase linearly with increasing heat flux.

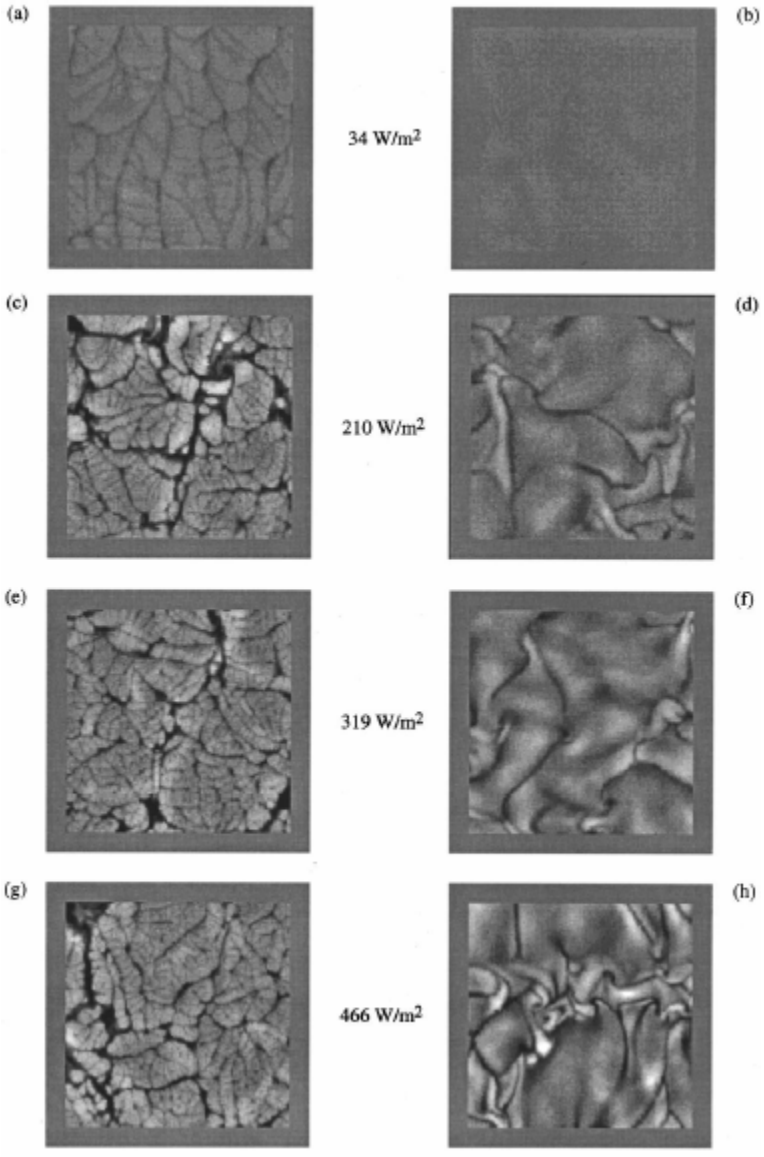

Figure 2.5: Temperature fields at various heat fluxes. The images on the left are clean systems (no surfactant) and the images on the right are systems covered with a monolayer of surfactant[18].

The same technique has been used to measure the spreading of contaminants on the surface of water[42, 45]. In Figure 2.6, the progression of film spreading is shown, starting at (a) when a drop of heptane/oleyl alcohol is shown just prior to being dropped. The expanding ring of contaminant clearly changes the surface structure of the water beneath. The IR thermography technique is reported to show the progression of the contaminant more effectively than shadowgraphic techniques previously used[46, 47]. The shadowgraphic techniques measure the curvature that develops on the surface as the contaminant flows across the surface. This technique is error prone for systems that are not extremely smooth.

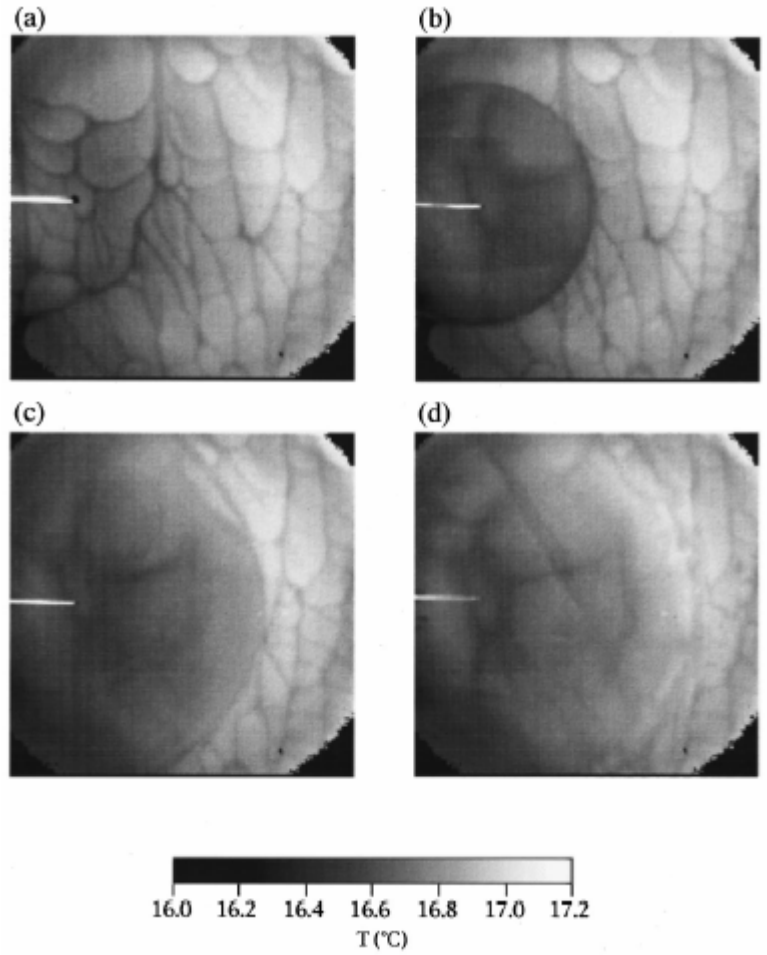

Figure 2.6: IR image showing the spread of surfactant on an evaporating water surface. Time between images is 250 milliseconds[45].

The ability to recognize contaminants with IR thermography has been extended to determining the local surface tension[48]. Surface tension measurements were made using the Wilhelmy plate technique across an image field. The surface tension results were then correlated with the IR images taken during the surface tension measurement and the IR images were found to be more revealing than the traditional surface tension measurement. This result could lead to an improved technique to measure the cleanliness of a liquid surface. In a recent article, Phongikaroon et al. report results using this

application to measure the role of contaminants and the temperature profile in the development of a Reynolds ridge wave structure[49].

3 EXPERIMENTAL RESULTS AND DISCUSSION

Experiments were designed to test the ability of IR thermography to recognize film breakage during drying by analyzing the COV temperature data. The first section will present data gathered during the drying of paper to show the strong dependence of the temperature readings on emissivity. The drying of wood chips is presented and followed by polymer adhesive film drying. Some of the results presented in this section have been published in Industrial & Engineering Chemistry Research and the article appears in Appendix B of this thesis[50].

Thermograms were taken with an AGEMA 900SW/TE system, comprised of an IR scanner equipped with a 40-degree FOV IR lens and a high-speed system controller. The scanner detects radiation in the mid-IR range (2-5.4 μm). The system is able to analyze images at the pixel level of resolution, and compensates for transmission through the atmosphere. The error in temperature measurement at 100 ^{o}C is 0.7 ^{o}C[19, 51]. Each experimental time increment has an individual temperature for each of the pixels within the area of interest. The numerical average of these numbers is the temperature of the area. The COV is calculated by dividing the standard deviation of all the temperatures in the area by the average temperature. The error bars provided on the graphs throughout this section represent one standard deviation of the experimental data. Error bars are not shown if the percent standard deviation was less than 5%.

The oven-camera set up is shown in Figure 3.1. Prior to each measurement, the oven door is closed until the oven heats to the set temperature. Following the heating, the samples are placed in the oven and recording of the IR signal is started.

Figure 3.1: Picture of the IR camera and oven used in the experiments.

The placement of the samples in the oven is shown in Figure 3.2. Thermal reflections from hot spots in the oven are blocked with the cardboard insert. The hot spots were originally responsible for deviations in the COV values. The ability of the cardboard to block the thermal reflections was evaluated by imaging the heating of a silicon wafer,

shiny side up and adjusting the cardboard to minimize the COV values. The average COV value for the heating of silicon without the cardboard was 0.004 compared to 0.002 for the heating with the cardboard.

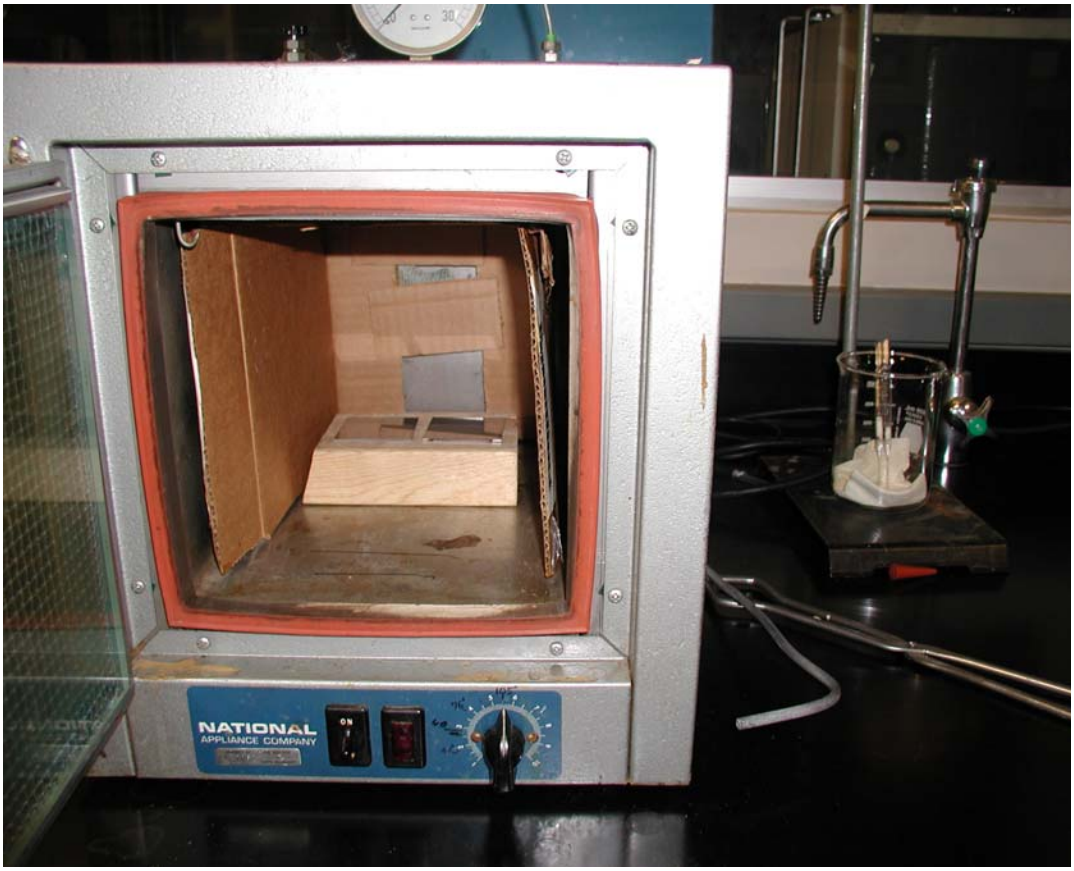

Figure 3.2: Picture of the placement of the samples in the oven and the cardboard enclosure used to block reflections of heat.

Data were extracted from the ThermaCAM Researcher 2000 system using a program written in Visual Basic for Applications within Excel. The code is in Appendix A. For each sample, the area was determined manually and the program exported the average

temperature, standard deviation, and time data into the Excel spreadsheet, which is where the data were manipulated and presented.

3.1 Dependence on Emissivity

As discussed in the literature review, temperature measurements made by IR thermography depend significantly on the value of emissivity chosen. To further demonstrate this strong dependence, not only on temperature but also on RMS temperature, the drying of paper was studied. The emissivity is reported to vary from 0.07 to 0.90, depending on the type of paper and the moisture content of the sheet[52].

The measurements were made using the IR camera to image the drying of a 64 g/m^2 sheet of bleached paper from 40% solids until it dries completely. The data were analyzed at three different emissivity (ε) values, 0.1, 0.5, and 0.9 that encompass the entire range of values reported for paper. Figure 3.3 shows the direct effect emissivity values have on temperature readings. Temperature differences of 60 ^oC are possible by changing the emissivity throughout its range.

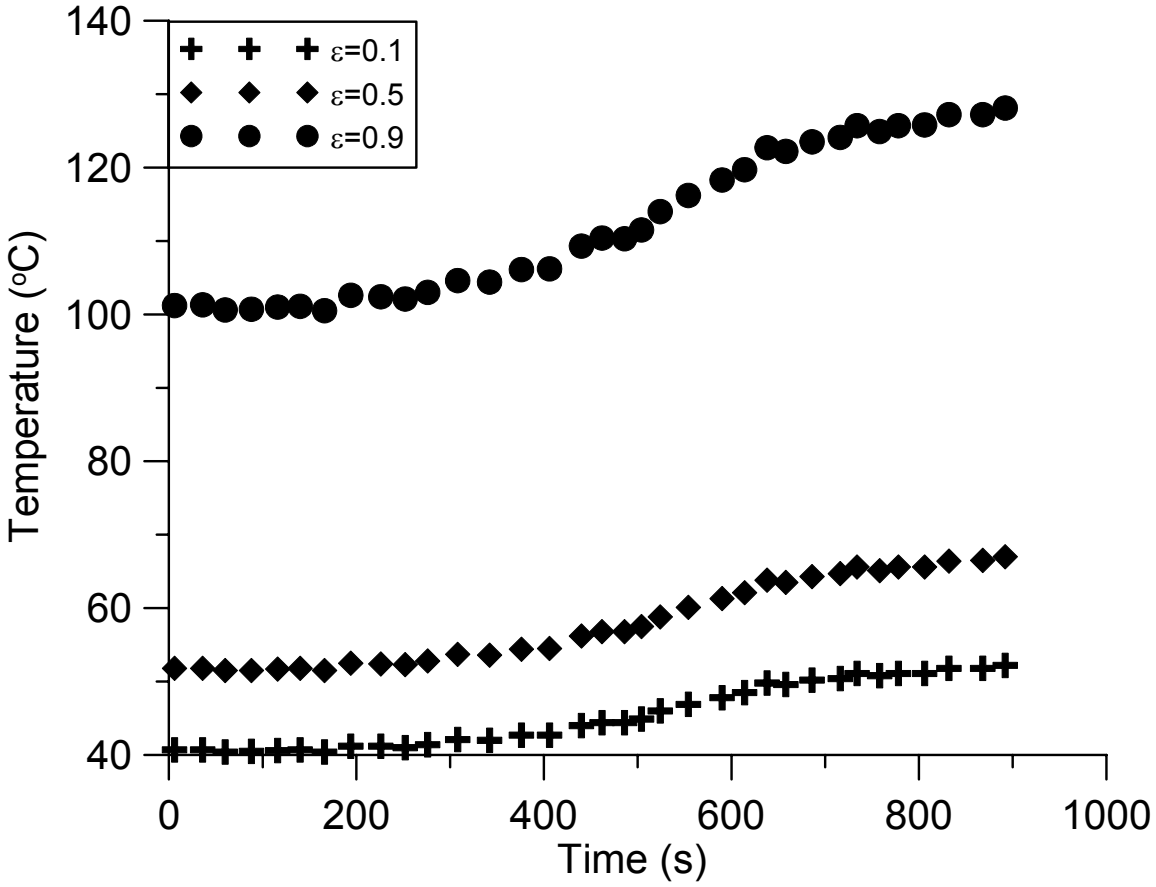

Figure 3.3: Temperature vs. time for the drying of paper at various emissivities.

Temperature differences from infrared images have been reported in the literature as RMS[18], which is also emissivity dependent as shown in Figure 3.4. Here, the magnitude of the temperature affects the RMS values significantly with potential errors near 300%.

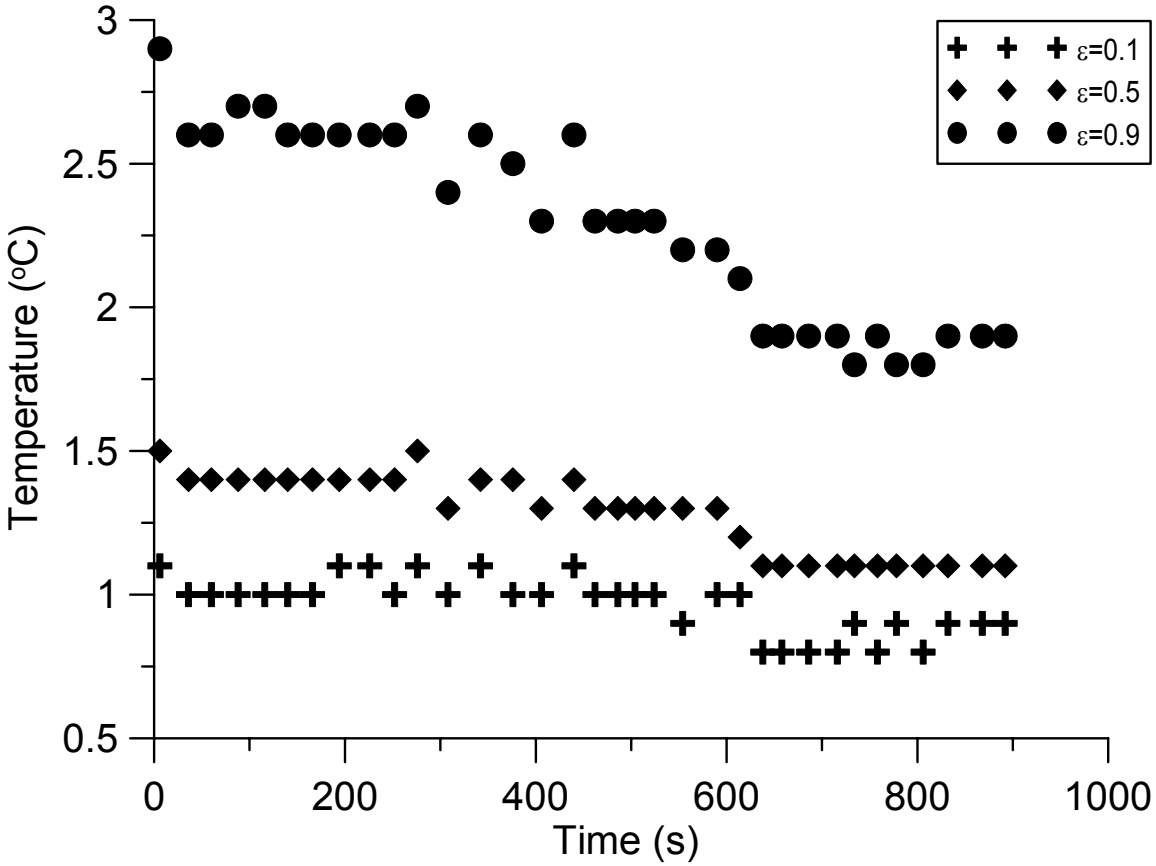

Figure 3.4: RMS temperature values vs. time for the drying of paper at various emissivities.

By computing the COV of the temperature profile of the image at each time interval, the dependence on emissivity is eliminated. Figure 3.5 shows the COV data for the three emissivity levels. The error in the measurements is on the order of the noise in the system as calculated by measuring the heating of a silicon wafer (~0.002).

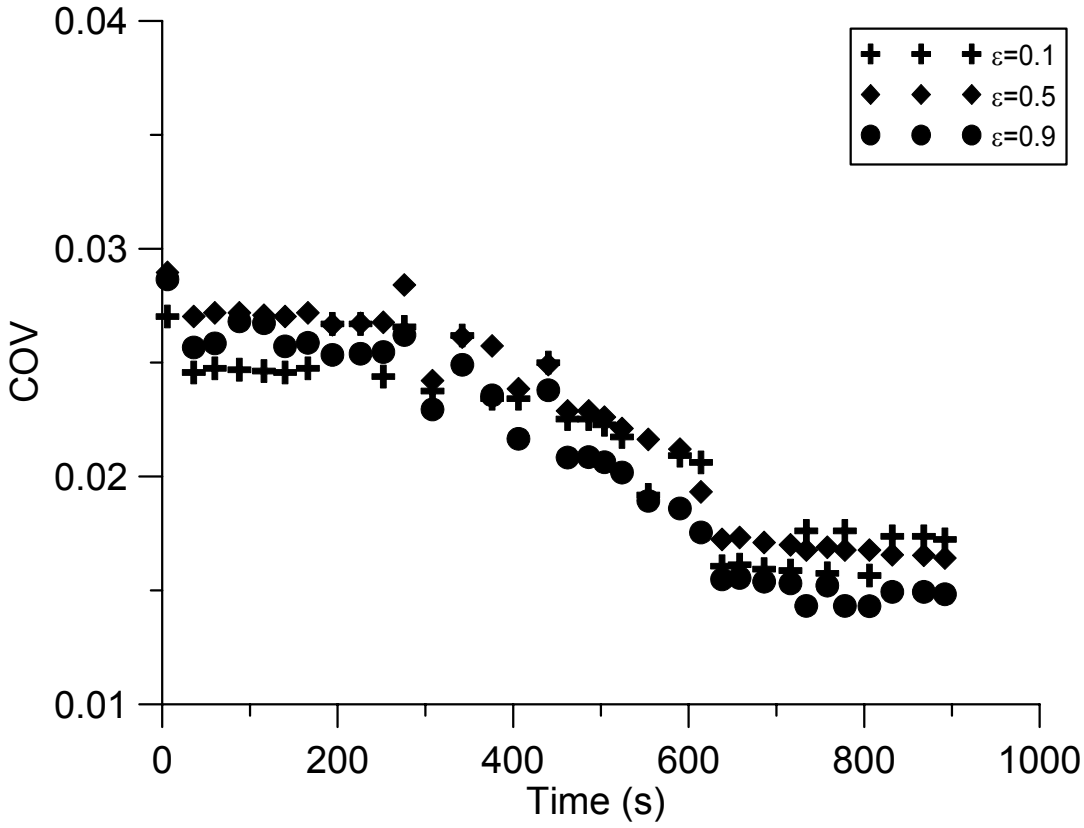

Figure 3.5: COV vs. time for the drying of paper at various emissivities.

The results of using the COV technique on two industrially interesting applications will be presented. The rate at which wood dries contributes to environmental emissions problems and the results from the COV technique will be used to characterize the drying process as it relates to emissions. Also, the tackiness of pressure sensitive adhesives (PSA) is dependent on the drying process. The COV technique will be used to correlate drying to finished product quality for a polyacrylate adhesive.

3.2 Study of Wood Drying

Pine and yellow poplar veneer were obtained from Georgia-Pacific and Potlatch, respectively. Pine flakes for the production of oriented strand board were provided by Georgia-Pacific. The veneer was cut into 12.7 x 8.9 x 0.42 cm pieces and oven-dried at different temperatures. The oven door was kept open and the focal plane of the scanner was set at 50 cm from the wood surface. Thermograms were taken every minute, after which the sample was quickly weighed and then replaced in the oven. An emissivity value of 0.92 was estimated by heating a sample of veneer and measuring its temperature with both a thermocouple and the IR camera. It was then adjusted until the IR-derived temperature corresponded to that obtained from the thermocouple. Flakes were imaged as single pieces. The moisture content (MC) of the wood samples was calculated on a dry basis as a percentage using the following equation[53]:

$$MC = \frac{w_w - w_{od}}{w_{od}} \times 100 , \qquad \textbf{Equation 3.1}$$

where, w_w is the weight of the wet wood and w_{od} is the weight of the oven dry wood.

When wood dries its water initially migrates to and evaporates from the surface. Evaporative cooling keeps the material at just below 100 ^{o}C regardless of dryer temperature[54]. As the surface begins to dry out, evaporative cooling ceases and the temperature starts to climb. If the dryer temperature is high enough the wood tissue can degrade and release methanol, formaldehyde and other hazardous air pollutants[55]. For softwood, the higher temperature increases the vapor pressure of terpenes and promotes

their emissions[54]. High temperature can also degrade the surface properties of the dried product [1, 56, 57]. Hence, a method that measures the point at which the surface begins to dry out should be useful for optimizing drying conditions and endpoints.

Thermograms were taken of veneer pieces as they dried in the oven. Typical plots of the COV of the surface temperature vs. moisture content are shown in Figure 3.6 for yellow poplar and pine; the traces are very similar. In both cases, the COV rises as the wood dries to an MC of about 10-15%. The wood surface is heterogenous, consisting of knots and earlywood and latewood bands, and differences in heat transfer to these regions would be emphasized as the surface water film thins; the COV should increase accordingly. The COVs in Figure 3.6 peak at about 10-15% MC and then decrease to a common value. It is very likely that the peak reflects the point at which dry spots begin to form on the surface, and all the following observations can be explained through this mechanism. The peaks occur at progressively higher wood moisture content with increasing temperature because diffusion of water to the surface cannot keep up with surface evaporation at the higher temperature. The COVs reach a common value when the wood is completely dry. The common COV value follows, since the surface reaches a more uniform temperature when differences in evaporative cooling are removed.

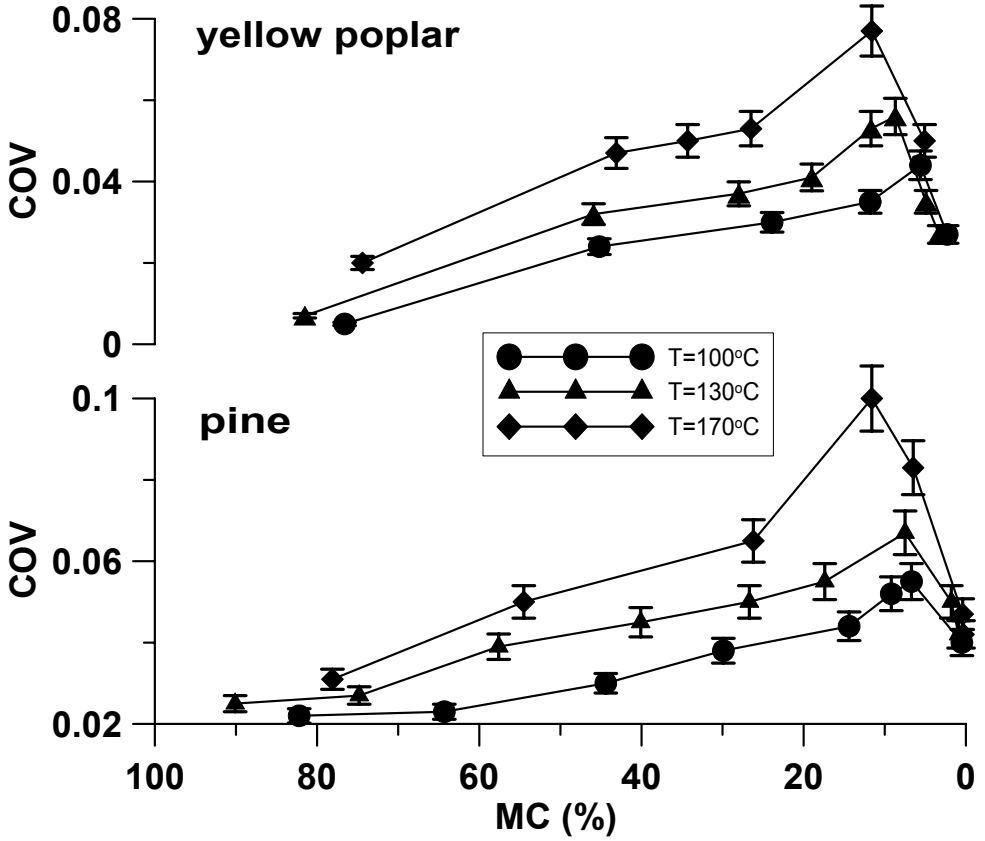

Figure 3.6: Dependence of the COV of the surface temperature on moisture content for veneer.

The relationship between temperature and MC is not sensitive enough to catch the onset of surface dryout, as shown in Figure 3.7 for pine; a similar temperature-MC profile was found for yellow poplar. This insensitivity is not surprising, because the average temperature will not change much at the point where dryout begins. The distribution of the surface temperature will be more strongly affected.

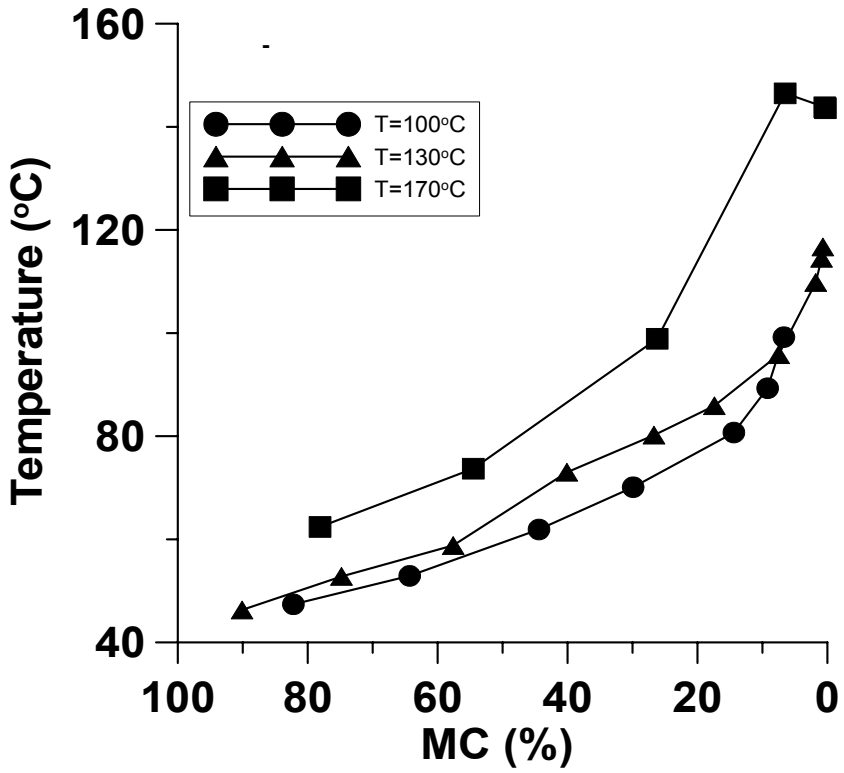

Figure 3.7: Variation of surface temperature with moisture content for pine veneer.

There is no attempt to relate the profiles in Figure 3.6 to the mechanism of water loss from wood. Below about 25% MC, the water in wood is sorbed to fiber, and the movement of this water is complex. The COV changes that occur at 15% MC in Figure 3.6 must, therefore, involve bound water.

Analogous data for drying individual pine flakes are illustrated in Figure 3.8. Flakes are thinner than veneer and proportionately less moisture resides in the smaller core. As a result, the position of the COV maximum occurs later at about 5% for the flakes, because surface dry out starts at a lower overall moisture content. The 5% threshold is environmentally significant. It has been previously found that the amounts of methanol

and formaldehyde released from flakes during commercial drying rise sharply when the flake MC drops below 5%[55]. It is reasoned that the surface starts to dry out at about 5% MC, and the subsequent temperature rise degrades wood tissue and leads to these emissions. The COV peak in Figure 3.8 provides independent evidence that surface dryout starts at about 5% MC.

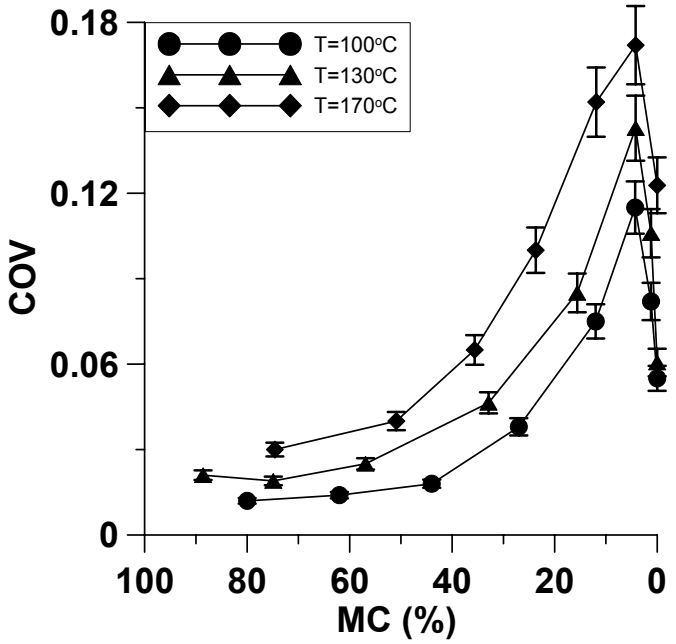

Figure 3.8: Dependence of the COV of the surface temperature on moisture content for pine flakes.

3.3 Deposition of Pressure Sensitive Adhesives

A commercial polyacrylate aqueous emulsion (obtained from Noveon, Inc. Cleveland, OH) was spread across 5 x 5 cm 304L stainless steel and 1008 carbon steel metal coupons using a wire-wrapped coating rod (R.D. Specialties, Inc., Webster, NY) that produces a constant meniscus and, therefore, an even coating. Prior to coating, the

coupons were mill-finished; profilometry confirmed that the RMS roughness values were equal for each of the metal samples. They were then cleaned with a sequence of solvents (acetone, methanol, isopropanol, and water) to remove any oils left from processing. The coated coupons were placed in the oven on a 2.5-cm thick piece of wood to isolate the coupons from the oven shelf. Images were taken every second during the drying of the polymer film, and these images were analyzed to determine the COV of the film during drying. The moisture content of the films was too small relative to the mass of the coupon for an accurate determination to be made.

The film thickness was varied from 4-40 μm and measured by a magnetic thickness probe (CMI International, now Oxford Instruments Measurement Systems LLC, Elk Grove Village, IL). The roughness of the dry films was determined using a MFP-3D AFM from Asylum Research (Santa Barbara, CA) equipped with AC240TS Silicon tips from Olympus (Japan). Topographic images for the films were determined using the AFM in the tapping mode. The cantilever/tip properties were as follows: spring constant – 1.2-2.1 N/m, resonance frequency – 75-82 kHz, tip shape – tetrahedral, and tip radius – 10 nm.

PSAs are widely used in the paper industry because of their ability to form strong bonds with short contact times and low pressures. Recent studies of the bonding process have reported that surface roughness of the film or substrate limits the total area available for bonding, thereby reducing the overall bond strength [58, 59]. Furthermore, studies on PSA debonding have identified surface roughness as an important variable responsible

for the development of nucleation sites that lead to cavities, which cause PSA bonds to fail [60]. Many PSAs are applied through use of a solvent, where the film deposits on the surface as the solvent evaporates. Irregularities in the film that develop during drying contribute to the roughness of the film, and it is, therefore, important to control film roughness as the polymer film is formed.

Measurements were made with films of two roughness levels. The RMS roughness values were 47.0 ± 0.2 nm and 40.2 ± 0.1 nm for the "rough" and "smooth" films, respectively. The corresponding peak-to-valley distances were 200 and 60 nm, respectively. Temperature profiles for drying the adhesive films at two oven temperatures are illustrated in Figure 3.9.

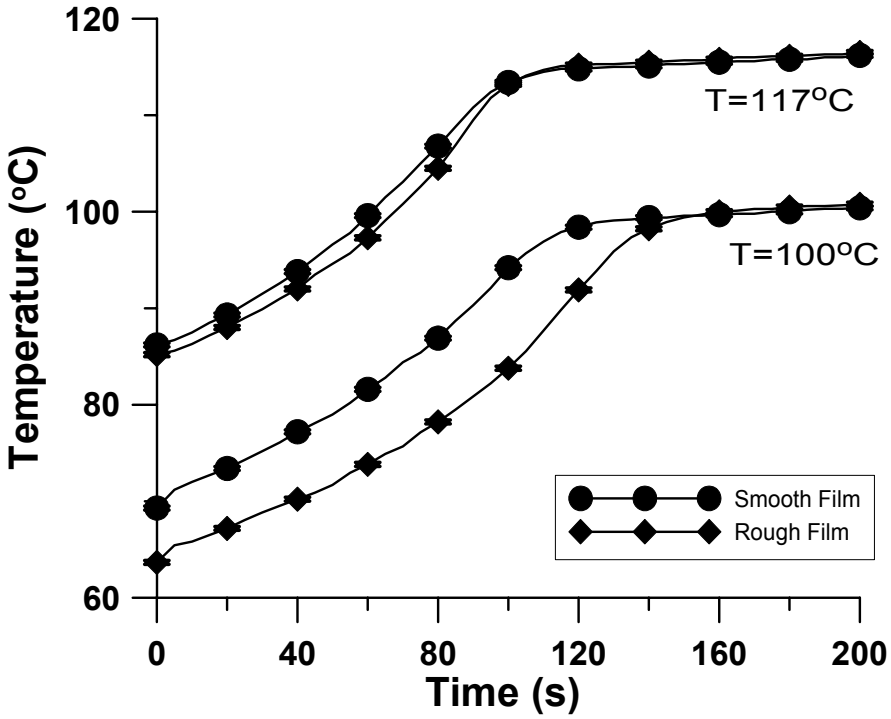

Figure 3.9: Variation of surface temperature with time for smooth and rough polyacrylate films at dryer temperatures of 100 °C and 117 °C.

The plot shows that the temperatures of the films increase and then level off as they approach the oven temperature. As with the analogous plot for wood, there is no indication of film breakage. A problem with using IR thermography to measure the absolute temperature of drying films is that the emissivity is highly dependent on the amount of water present in the film[19]. As the film dries and the emissivity changes, the measurement of the absolute temperature is difficult. This changing emissivity can contribute to the differences in film temperature during heating as shown in Figure 3.9. An advantage of using the COV technique to analyze materials with changing emissivity

is that the division of two temperature-dependent terms eliminates emissivity from the calculation.

The COV plots in Figure 3.10 are for drying at 117 ^{o}C. The upper curve is for the rough surface. The COV starts at a higher value because the film is thicker and heat transfer to a rough surface is more variable than to a smooth one. The COV then falls sharply and reaches a value close to that for the smoother surface. This must mean that the film breaks at this point where the COV drops. The lower curve in Figure 3.10 represents COV data for the smooth film. The magnitude of the COV is lower for this surface, possibly because the film is more uniform, surface irregularities are smaller, and the temperature and COV of the film are more closely equivalent to that of the underlying metal surface. The profile of the smooth film displays only a slight rise prior to a drop in value to the equilibrium value.

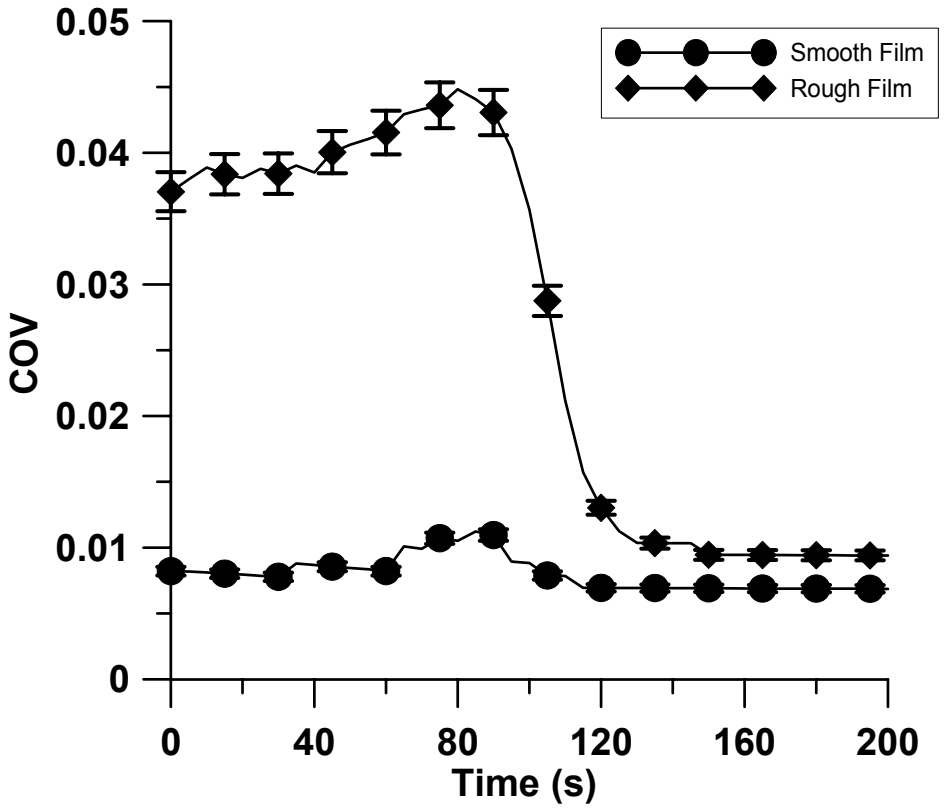

Figure 3.10: Dependence of the COV of the surface temperature on time during the drying of a polyacrylate film at 117 ^{o}C.

Figure 3.11 illustrates COV profiles at 100 ^{o}C. The COV for the rough surface is much more regular throughout because the lower temperature allows moisture to redistribute[61] and promote more uniform drying. Although at a lower magnitude, similar features are present in the curves at the lower temperature. Background noise in the measurement was considered by analyzing the COV profiles during heating of a silicon wafer. The silicon wafer, very uniform in composition and heat transfer properties, produced very small (~0.002) COV values during heating. These COV profiles for the metal surfaces contrast with those for wood where the COV first rises,

because the wood surface is much rougher than that of a metal surface and differences in heat transfer are accentuated.

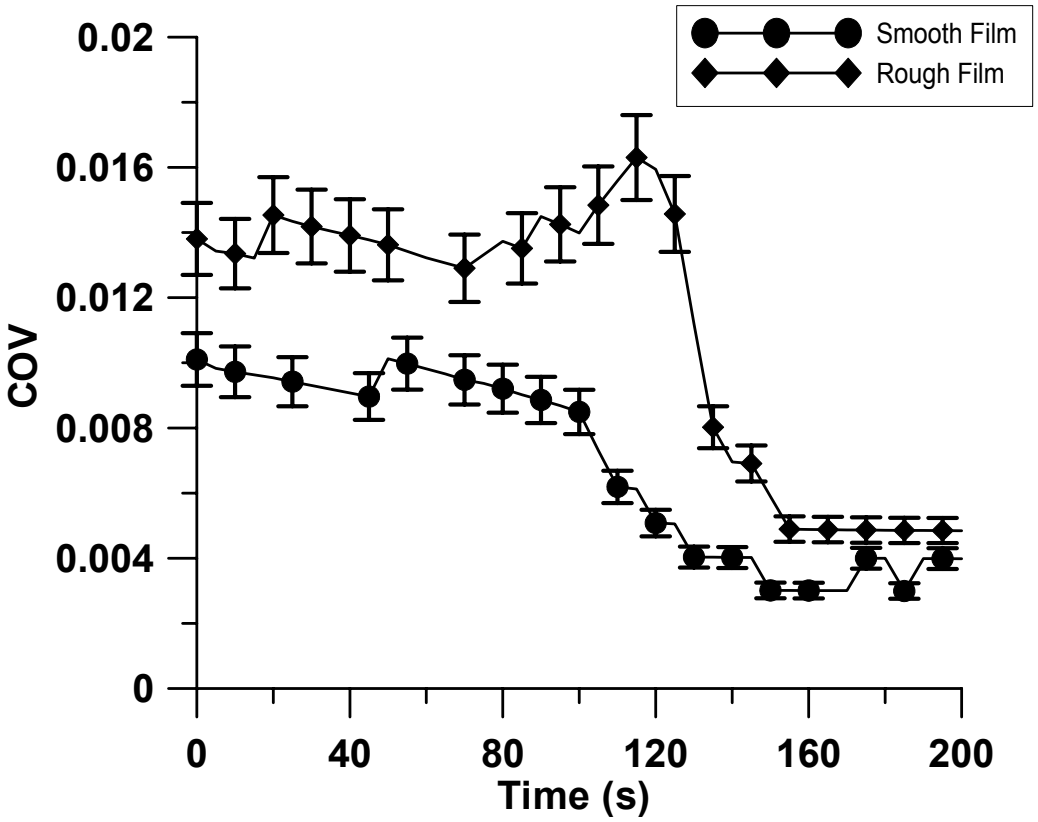

Figure 3.11: Dependence of the COV of the surface temperature on time during the drying of a polyacrylate film at 100 ^{o}C.

3.4 Conclusions

In summary, COV analysis of IR thermography provides a method of visualizing the breakage of a liquid film on metal coupons or the onset of dryout for wood surfaces during drying. The COV analysis is much more sensitive than measuring the average temperature of the film during drying and is able to indicate the point at which the film

breaks and the subsequent lack of evaporative cooling allows the dry spots to warm. Also, small differences in heat transfer caused by surface irregularities can be detected.

By dividing two temperature terms, the role of emissivity is eliminated from the measurement, which is useful for measurements of materials while they dry. Often, during drying, the emissivity of the materials changes drastically, making traditional thermography problematic. Because of this utility, the technique should be useful in the design and monitoring of processes where film dewetting is important.

Appendix A – VBA Program to Extract Data from IR Application

```
Sub PlaySequence_Click()
   Dim sess As Object
   Dim row As Integer
   Dim col As Integer
   row = 15
   col = 2
   ' Get a reference to the ThermaCAM Researcher object
   Set sess = _
     Worksheets("Sheet4").OLEObjects("Object 1").Object
   ' Move to the first image in the session
   sess.GotoFirstImage

   ' Start a loop that iterates through all images
   ' in the session
   Do While True
      ' Store IR image time and spotmeter temperatures

      ' in the cells
      Worksheets(4).Cells(row, col).Value = _
        sess.GetNamedValue("ar1.avg")
      Worksheets(4).Cells(row, col + 1).Value = _
        sess.GetNamedValue("ar1.stdev")
      Worksheets(4).Cells(row, col + 2).Value = _
        sess.GetNamedValue("ar2.avg")
      Worksheets(4).Cells(row, col + 3).Value = _
        sess.GetNamedValue("ar2.stdev")
      'Record time in first column
      '
      Worksheets(4).Cells(row, col + 4).Value = _
        sess.GetNamedValue("time")

      If sess.IsLastImage Then
        Exit Do
      End If
      ' Load next image in the session and

      ' increment the row counter
      sess.StepForward
      row = row + 1
   Loop

End Sub
```

Appendix B – COV PAPER PUBLISHED IN I&ECR

Reproduced with permission from Fike, G., J. Abedi, and S. Banerjee, *Imaging the Drying of Surfaces by Infrared Thermography.* Ind. Eng. Chem. Res., 2004. **43**: p. 4178-4181. Copyright 2004 American Chemical Society.

Imaging the Drying of Surfaces by Infrared Thermography

Gregory M. Fike, Jalal Abedi, and Sujit Banerjee*

Institute of Paper Science and Technology and School of Chemical & Biomolecular Engineering, Georgia Institute of Technology, 500 Tenth Street NW, Atlanta, Georgia 30332-0620

Infrared (IR) thermography was used to monitor the drying of water from both smooth and rough surfaces. An analysis using the coefficient of variance (COV) of the temperature shows the point at which surface dryout begins. The dry spots that develop on a surface lead to temperature variations across the surface. The COV reflects these variations and is a sensitive measure of the early stages of dryout. The shape of the COV profile as the surface approaches dryness depends on the roughness of the surface. For rough surfaces such as wood, the COV climbs because differences in heat transfer to the heterogeneous wood surface are accentuated. Changes in the COV are much smaller for polymer films deposited on metal surfaces but are still dependent upon surface roughness.

Introduction

The manner in which a solvent evaporates from a surface can control the properties of the dried surface. For instance, when wood flakes are dried for the manufacture of oriented strand board, the evenness of drying impacts the surface properties of the flakes and can affect the strength of the adhesive bond when the flakes are subsequently glued together.[1] In another example, when a film is deposited from a solvent, the uniformity and topology of the film can be influenced by the rate of evaporation. These properties are important in many applications,[2−6] and topology is often measured after deposition with techniques such as atomic force microscopy (AFM),[3,7,8] scanning force microscopy,[9] transmission electron microscopy,[7] and optical microscopy.[7,8,10] Less common are techniques such as laser interferometry, shadowgraphy, and optical microscopy, where the film is monitored while it forms.[10,11]

Infrared (IR) thermography has been used as a tool in a number of applications in heat transfer,[12] fluid dynamics,[13] and corrosion.[14] In principle, IR thermography can detect the point at which surface dryout begins because evaporative cooling is lost at this point and the surface temperature rises. However, the temperature rise is initially quite small and can be difficult to detect. The coefficient of variance (COV) of the temperature (defined as the standard deviation of temperature divided by the average temperature) can detect the onset of surface dryout with greater sensitivity. The surface is now exposed in spots, which increases the temperature variations across the surface. The COV reflects these variations and is, therefore, a much more sensitive measure of the early stages of liquid film breakage than is the average surface temperature. Also, by division of two temperature terms, changes in the emissivity of the surface during drying are eliminated. This is beneficial in cases either where the emissivity of the material is unknown or where it changes, e.g., because of the evaporation of water or oxidation of the surface during measurement.[15]

In this paper we demonstrate the technique with two applications: wood drying, where the surface is rough, and the deposition of an organic film from water on a smooth metal surface. The COV of the surface temperature is able to cleanly identify the point at which the surface begins to dry out or when the surface film breaks.

Experimental Section

Thermograms were taken with an AGEMA 900SW/TE system, comprised of an IR scanner equipped with a 40° field-of-view IR lens and a high-speed system controller. The scanner detects radiation in the 2−5.4 μm range. The system is able to analyze images at the pixel level of resolution and compensates for transmission through the atmosphere. The error in temperature measurement at 100 °C is 0.7 °C.[15,16] Each experimental time increment has an individual temperature for each of the pixels within the area of interest. The numerical average of these numbers is the temperature of the area. The COV is calculated by dividing the standard deviation of all of the temperatures in the area by the average temperature. The error bars provided on the graphs represent 1 standard deviation of the experimental data. Error bars are not shown if the percent standard deviation was less than 5%.

Pine and yellow poplar veneer were obtained from Georgia-Pacific and Potlatch, respectively. Pine flakes for the production of oriented strand board were provided by Georgia-Pacific. The veneer was cut into 12.7 × 8.9 × 0.42 cm pieces and oven-dried at different temperatures. The oven door was kept open, and the focal plane of the scanner was set at 50 cm from the wood surface. Thermograms were taken every 1 min, after which the sample was quickly weighed and then replaced in the oven. An emissivity value of 0.92 was estimated by heating a sample of veneer and measuring its temperature with both a thermocouple and the IR scanner. It was then adjusted until the IR-derived temperature corresponded to that obtained from the thermocouple. Flakes were imaged as single pieces. The moisture content (MC) of the wood samples was calculated on a dry basis as a percentage using the following equation:[17]

$$\mathrm{MC} = \frac{W_w - W_{od}}{W_{od}} \times 100$$

where W_w is the weight of the wet wood and W_{od} is the weight of the oven-dried wood.

10.1021/ie0343364 CCC: $27.50 © 2004 American Chemical Society
Published on Web 06/09/2004

A commercial polyacrylate aqueous emulsion (obtained from Noveon, Inc., Cleveland, OH) was spread across 5 × 5 cm, 304 L stainless steel and 1008 carbon steel metal coupons using a wire-wrapped coating rod (R.D. Specialties, Inc., Webster, NY) that produces a constant meniscus and, therefore, an even coating. Prior to coating, the coupons were mill-finished; profilometry confirmed that the root-mean-square (rms) roughness values were equal for each of the metal samples. They were then cleaned with a sequence of solvents (acetone, methanol, 2-propanol, and water) to remove any oils left over from processing. The coated coupons were placed in the oven on a 2.5-cm-thick piece of wood to isolate the coupons from the oven shelf. Images were taken every 1 s during the drying of the polymer film, and these images were analyzed to determine the COV of the film during drying. The MC of the films was too small relative to the mass of the coupon for an accurate determination to be made.

The film thickness was varied from 4 to 40 μm and measured by a magnetic thickness probe (CMI International, now Oxford Instruments Measurement Systems LLC, Elk Grove Village, IL). The roughness of the dry films was determined using a MFP-3D atomic force microscope (AFM) from Asylum Research (Santa Barbara, CA) equipped with AC240TS Si tips from Olympus (Japan). Topographic images for the films were determined using the AFM in the tapping mode. The cantilever/tip properties were as follows: spring constant (k), 1.2−2.1 N/m; resonance frequency, 75−82 kHz; tip shape, tetrahedral, and tip radius, 10 nm.

Results and Discussion

Wood Drying. When wood dries, its water initially migrates to and evaporates from the surface. Evaporative cooling keeps the material at just below 100 °C regardless of the dryer temperature.[18] As the surface begins to dry out, evaporative cooling ceases and the temperature starts to climb. If the dryer temperature is high enough, the wood tissue can degrade and release methanol, formaldehyde, and other hazardous air pollutants.[19] For softwood, the higher temperature increases the vapor pressure of terpenes and promotes their emissions.[18] High temperature can also degrade the surface properties of the dried product.[1,20,21] Hence, a method that measures the point at which the surface begins to dry out should be useful for optimizing drying conditions and end points.

Thermograms were taken of veneer pieces as they dried in the oven. Typical plots of the COV of the surface temperature vs MC are shown in Figure 1 for yellow poplar and pine; the traces are very similar. In both cases, the COV rises as the wood dries to an MC of about 10−15%. The wood surface is heterogeneous, consisting of knots and earlywood and latewood bands, and differences in heat transfer to these regions would be emphasized as the surface water film thins; the COV should increase accordingly. The COVs in Figure 1 peak at about 10−15% MC and then decrease to a common value. It is very likely that the peak reflects the point at which dry spots begin to form on the surface, and all of the following observations can be explained through this mechanism. The peaks occur at progressively higher wood moisture with increasing temperature because diffusion of water to the surface cannot keep up with surface evaporation at the higher temperature. The COVs reach a common value when the wood is completely dry. This follows because the surface reaches a more uniform temperature when differences in evaporative cooling are removed. The relationship between the temperature and MC is not sensitive enough to pick up the onset of surface dryout, as shown in Figure 2 for pine; a similar temperature−MC profile was found for yellow poplar. This insensitivity is not surprising because the average temperature will not change much at the point where dryout begins. The distribution of the surface temperature will be more strongly affected. We do not attempt to relate the profiles in Figure 1 to the mechanism of water loss from wood. Below about 25% MC, the water in wood is sorbed to the fiber and the movement of this water is complex. The COV changes that occur at 15% MC in Figure 1 must, therefore, involve bound water.

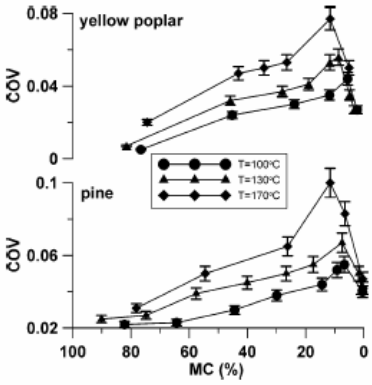

Figure 1. Dependence of the COV of the surface temperature on MC for veneer.

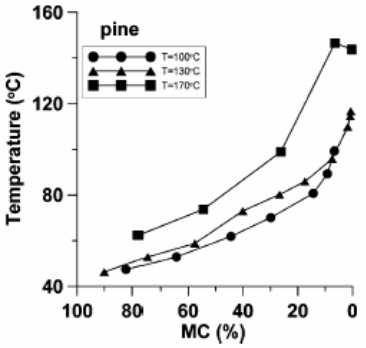

Figure 2. Variation of the surface temperature with MC for pine veneer.

Analogous data for drying individual pine flakes are illustrated in Figure 3. Flakes are thinner than veneer and proportionately less moisture resides in the smaller core. As a result, the position of the COV maximum occurs later at about 5% for the flakes, because surface dryout starts at a lower overall MC. The 5% threshold is environmentally significant. We previously found that the amounts of methanol and formaldehyde released from flakes during commercial drying rise sharply when the flake MC drops below 5%.[19] We reasoned that the surface starts to dry out at about 5% MC, and the subsequent temperature rise degrades wood tissue and leads to these emissions. The COV peak in Figure 3 provides independent evidence that surface dryout starts at about 5% MC.

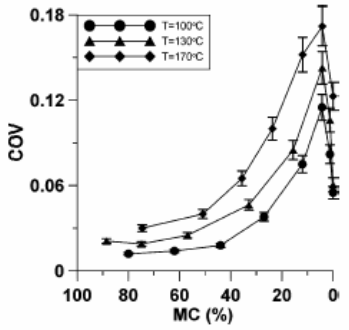

Figure 3. Dependence of the COV of the surface temperature on MC for pine flakes.

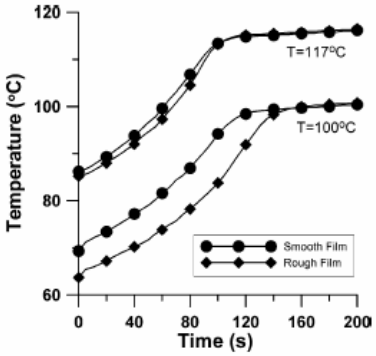

Figure 4. Variation of the surface temperature with time for smooth and rough polyacrylate films at dryer temperatures of 100 and 117 °C.

Deposition of Pressure-Sensitive Adhesives (PSAs). PSAs are widely used in the paper industry because of their ability to form strong bonds with short contact times and low pressures. Recent studies of the bonding process have reported that surface roughness of the film or substrate limits the total area available for bonding, thereby reducing the overall bond strength.[22,23] Furthermore, studies on PSA debonding have identified surface roughness as an important variable responsible for the development of nucleation sites that lead to cavities, which cause PSA bonds to fail.[24] Many PSAs are applied through use of a solvent, where the film deposits on the surface as the solvent evaporates. Irregularities in the film that develop during drying contribute to the roughness of the film, and it is, therefore, important to control film roughness as the polymer film is formed.

Measurements were made with films of two roughness levels. The rms roughness values were 47.0 ± 0.2 and 40.2 ± 0.1 nm for the "rough" and "smooth" films, respectively. The corresponding peak-to-valley distances were 200 and 60 nm, respectively. Temperature profiles for drying of the adhesive films at two dryer temperatures are illustrated in Figure 4. The plot shows that the temperatures of the films increase and then level off as they approach the oven temperature. As with the analogous plot for wood, there is no indication of film breakage. A problem with using IR thermography to measure the absolute temperature of drying films is that the emissivity is highly dependent on the amount of water present in the film.[15] As the film dries and the emissivity changes, the measurement of the absolute temperature is difficult. This changing emissivity can contribute to the differences in the film temperature during heating as shown in Figure 4. An advantage of using the COV technique to analyze materials with changing emissivity is that the division of two temperature-dependent terms eliminates emissivity from the calculation.

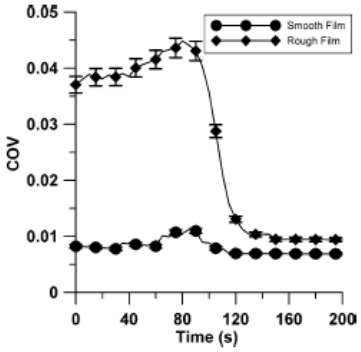

Figure 5. Dependence of the COV of the surface temperature on time during the drying of a polyacrylate film at 117 °C.

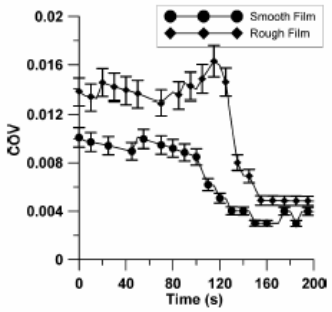

Figure 6. Dependence of the COV of the surface temperature on time during the drying of a polyacrylate film at 100 °C.

The COV plots in Figure 5 are for drying at 117 °C. The upper curve is for the rough surface. The COV starts at a higher value because the film is thicker and heat transfer to a rough surface is more variable than that to a smooth one. The COV then falls quite sharply and reaches a value close to that for the smoother surface. This must mean that the film breaks at this point where the COV drops. The lower curve in Figure 5 represents COV data for the smooth film. The magnitude of the COV is lower for this surface, possibly because the film is more uniform, surface irregularities are smaller, and the temperature and COV of the film are more closely equivalent to those of the underlying metal surface. The profile of the smooth film displays only a slight rise prior to a drop in value to the equilibrium value.

Figure 6 illustrates COV profiles at 100 °C. The COV for the rough surface is much more regular throughout because the lower temperature allows moisture to redistribute[25] and promote more uniform drying. Background noise in the measurement was considered by analyzing the COV profiles during heating of a silicon wafer. The silicon wafer is very uniform in composition and heat-transfer properties and produced very small (<0.002) COV values during heating. These COV profiles for the metal surfaces contrast with those for wood where the COV first rises, because the wood surface is very much rougher than the metal surface and differences in heat transfer are accentuated.

In summary, COV analysis of IR thermography provides a method of visualizing the breakage of a liquid film on metal coupons or the onset of dryout for wood surfaces during drying. Small differences in heat transfer caused by surface irregularities can be detected. The technique should be useful in the design and monitoring of processes where film dewetting is important.

Acknowledgment

We thank Georgia-Pacific, Potlatch, and the Electric Power Research Institute for financial support.

Literature Cited

(1) Martino, C.; Shrauti, S.; Banerjee, S.; Otwell, L.; Price, E. Flake drying temperature affects mat properties during pressing. *Holzforschung* **2002**, *56*, 558−562.

(2) Walheim, S.; Schaffer, E.; Mlynek, J.; Steiner, U. Nanophase-Separated Polymer Films as High-Performace Antireflection Coatings. *Science* **1999**, *283*, 520.

(3) Budkowski, A.; Bernasik, A.; Cyganik, P.; Raczkowska, J.; Penc, B.; et al. Substrate-Determined Shape of Free Surface Profiles in Spin-Cast Polymer Blend Films. *Macromolecules* **2003**, *36*, 4060−4067.

(4) Fanton, X.; Cazabat, A.; Quere, D. Thickness and Shape of Films Driven by a Marangoni Flow. *Langmuir* **1996**, *12*, 5875−5880.

(5) Routh, A.; Russel, W. Deformation Mechanisms during Latex Film Formation: Experimental Evidence. *Ind. Eng. Chem. Res.* **2001**, *40*, 4302−4308.

(6) Ghannam, M. Effect of Binders on the Flow Behavior of a Paper Coating Suspension over a Wide Range of Shear Rates. *Ind. Eng. Chem. Res.* **2002**, *41*, 2399−2404.

(7) Sharma, S.; Rafailovich, M.; Peiffer, D.; Sokolov, J. Control of Dewetting Dynamics by Adding Nanoparticle Fillers. *Nano Lett.* **2001**, *1*, 511−514.

(8) Lee, S.-H.; Kang, H.; Youn, S.; Char, K. Hierarchical Surface Topography in Block Copolymer Thin Films Induced by Residual Solvent. *Macromolecules* **2003**, *36*, 4907−4915.

(9) Mertig, M.; Thiele, U.; Bradt, J.; Klemm, D.; Pompe, W. Dewetting of thin collagenous precursor films. *Appl. Phys. A* **1998**, *66*, S565−S568.

(10) Schwartz, L.; Roy, R.; Eley, R.; Petrash, S. Dewetting Patterns in a Drying Liquid Film. *J. Colloid Interface Sci.* **2001**, *234*, 363−374.

(11) Grigoriev, R. Control of evaporatively driven instabilities of thin liquid films. *Phys. Fluids* **2002**, *14*, 1895−1909.

(12) Theofanous, T. G.; Tu, J. P.; Dinh, A. T.; Dinh, T. N. The boiling crisis phenomenon Part I: nucleation and nucleate boiling heat transfer. *Exp. Therm. Fluid Sci.* **2002**, *26*, 775−792.

(13) Carlomagno, G. M.; Astarita, T.; Cardone, G. Thermographic Investigation of Some Surface Flow Patterns. *J. Visualization* **2000**, *2*, 381−393.

(14) Han, J.-S.; Park, J.-H. Detection of corrosion steel under an organic coating by infrared photography. *Corros. Sci.* **2004**, *46*, 787−793.

(15) *Thermovision 900 series user's manual*; AGEMA Infrared Systems: Danderyd, Sweden, 1993.

(16) Incropera, F.; DeWitt, D. *Fundamentals of heat and mass transfer*, 4th ed.; Wiley: New York, 1996.

(17) Bierman, C. *Handbook of Pulping and Papermaking*, 2nd ed.; Academic Press: San Diego, CA, 1996.

(18) Banerjee, S.; Su, W.; Otwell, L.; Hittmeier, M.; Nichols, K. Wet line extension reduces VOCs from softwood drying. *Environ. Sci. Technol.* **1998**, *32*, 1303−1307.

(19) Su, W.; Yan, H.; Banerjee, S.; Otwell, L.; Hittmeier, M. Field-proven strategies for reducing VOCs from hardwood drying. *Environ. Sci. Technol.* **1999**, *33*, 1056−1059.

(20) Christiansen, A. How overdrying wood reduces its bonding to phenol−formaldehyde adhesives: a critical review of the literature. Part I. Physical responses. *Wood Fiber Sci.* **1990**, *22*, 441−459.

(21) Christiansen, A. How overdrying wood reduces its bonding to phenol−formaldehyde adhesives: a critical review of the literature. Part II. Chemical reactions. *Wood Fiber Sci.* **1991**, *23*, 69−84.

(22) Creton, C.; Leibler, L. How does tack depend on time of contact and contact pressure? *J. Polym. Sci. B* **1996**, *34*, 545−554.

(23) Creton, C.; Fabre, P. T. The Mechanics of Adhesion, Rheology of Adhesives, and Strength of Adhesive Bonds. In *Surfaces, Chemistry and Applications*; Elsevier: Amsterdam, 2002; Vol. 1.

(24) Chiche, A.; Pareige, P.; Creton, C. Role of surface roughness in controlling the adhesion of a soft adhesive on a hard surface. *C. R. Acad. Sci. Paris* **2000**, *IV*, 1197−1204.

(25) Ahrens, F.; Hojjatie, B.; Coffin, D. Influence of Drying Variables in Development of Cockle: An Experimental Study. *International Paper Physics Conference*; TAPPI & PAPTEC: Victoria, British Columbia, Canada, 2003; pp 137−142.

Received for review December 22, 2003
Revised manuscript received March 31, 2004
Accepted May 5, 2004

IE0343364

REFERENCES

1. Martino, C., S. Shrauti, S. Banerjee, L. Otwell, and E. Price, *Flake drying temperature affects mat properties during pressing.* Holzforschung, 2002. **56**: p. 558-562.

2. Walheim, S., E. Schaffer, J. Mlynek, and U. Steiner, *Nanophase-Separated Polymer Films as High-Performace Antireflection Coatings.* Science, 1999. **283**(5401): p. 520.

3. Budkowski, A., A. Bernasik, P. Cyganik, J. Raczkowska, B. Penc, B. Bergues, K. Kowalski, J. Rysz, and J. Janik, *Substrate-Determined Shape of Free Surface Profiles in Spin-Cast Polymer Blend Films.* Macromolecules, 2003. **36**: p. 4060-4067.

4. Fanton, X., A. Cazabat, and D. Quere, *Thickness and Shape of Films Driven by a Marangoni Flow.* Langmuir, 1996. **12**: p. 5875-5880.

5. Routh, A. and W. Russel, *Deformation Mechanisms during Latex Film Formation: Experimental Evidence.* Ind. Eng. Chem. Res., 2001. **40**: p. 4302-4308.

6. Ghannam, M., *Effect of Binders on the Flow Behavior of a Paper Coating Suspension over a Wide Range of Shear Rates.* Ind. Eng. Chem. Res., 2002. **41**: p. 2399-2404.

7. Sharma, S., M. Rafailovich, D. Peiffer, and J. Sokolov, *Control of Dewetting Dynamics by Adding Nanoparticle Fillers.* Nano Letters, 2001. **1**(10): p. 511-514.

8. Lee, S.-H., H. Kang, S. Youn, and K. Char, *Hierarchical Surface Topography in Block Copolymer Thin Films Induced by Residual Solvent.* Macromolecules, 2003. **36**: p. 4907-4915.

9. Mertig, M., U. Thiele, J. Bradt, D. Klemm, and W. Pompe, *Dewetting of thin collagenous precursor films.* Appl. Phys. A., 1998. **66**: p. S565-S568.

10. Schwartz, L., R. Roy, R. Eley, and S. Petrash, *Dewetting Patterns in a Drying Liquid Film.* J. of Colloid and Interface Science, 2001. **234**: p. 363-374.

11. Grigoriev, R., *Control of evaporatively driven instabilities of thin liquid films.* Physics of Fluids, 2002. **14**(6): p. 1895-1909.

12. Theofanous, T.G., J.P. Tu, A.T. Dinh, and T.N. Dinh, *The boiling crisis phenomenon Part I: nucleation and nucleate boiling heat transfer.* Experimental Thermal and Fluid Science, 2002. **26**: p. 775-792.

13. Theofanous, T.G., A.T. Dinh, J.P. Tu, and T.N. Dinh, *The boiling crisis phenomenon Part II: dryout dynamics and burnout.* Experimental Thermal and Fluid Science, 2002. **26**: p. 793-810.

14. Carlomagno, G.M., G. Cardone, C. Meola, and T. Astarita, *Infrared Thermography as a Tool for Thermal Surface Flow Visualization.* Journal of Visualization, 1998. **1**(1): p. 37-50.

15. Carlomagno, G.M., T. Astarita, and G. Cardone, *Thermographic Investigation of Some Surface Flow Patterns.* Journal of Visualization, 2000. **2**(3/4): p. 381-393.

16. Han, J.-S. and J.-H. Park, *Detection of corrosion steel under an organic coating by infrared photography.* Corrosion Science, 2004. **46**: p. 787-793.

17. Birnie, D., B. Zelinski, and D. Perry, *Infrared observation of evaporative cooling during spin-coating processes.* Optical Engineering, 1995. **34**(6): p. 1782-1787.

18. Saylor, J., G. Smith, and K. Flack, *An experimental investigation of the surface temperature field during evaporative convection.* Physics of Fluids, 2001. **13**(2): p. 428-439.

19. Thermovision, *900 series user's manual, AGEMA Infrared Systems*. 1993: Danderyd, Sweden.

20. Mitchell, C., *Thermography is Accurate Tool, Aids in Preventative Maintenance.* Pulp and Paper, 1987. **61**(13): p. 130-131.

21. Kaplan, H., *Practical applications of infrared thermal sensing and imaging equipment, 2nd Ed.* 1999, Bellingham, Washington USA: SPIE Optical Engineering.

22. Kimmitt, M., *Far-Infrared Techniques*. 1970, Bristol, Great Britain: J.W. Arrowsmith Limited.

23. Davey, H., *E&M spectrum*.

24. Weisstein, E., *Kirchhoff's Law*, Treasure Troves.

25. Holst, G., *Testing and evaluation of infrared imaging systems 2nd ed.* 1998, Bellingham, Washington USA: SPIE Optical Engineering Press.

26. McCarthy, D., *IR sensing*, Stanford.

27. Vanzetti, R., *Pratical Applications of Infrared Techniques*. 1972, New York: Wiley-Interscience.

28. Kemp, B., *Modern Infrared Technology*. 1962, Indianapolis, Indiana: Howard W. Sams & Co.

29. Cassis, L., *Near-infrared and infrared imaging analysis of lipid metabolism and energy expenditure*.

30. Wright, H., *Infrared techniques*. 1973, Oxford: Clarendon Press.

31. Atkins, J., *More uses for thermography around the mill.* Tappi J., 1982. **65**(11): p. 131-132.

32. Egnell, G. and G. Orlander, *Using infrared thermography to assess viability of Pinus sylvestris (scotch pine) and Picea abies (norway spruce) seedlings before planting.* Canadian J. of Forestry Research, 1993. **23**(9): p. 1737-1743.

33. Grant, A., *Infrared thermography -- a maintenance tool.* Paper Technology Industry, 1989. **30**(5): p. 19-20.

34. Mercer, C., *Thermography can help to improve paper machine efficiency.* Pulp and Paper Canada, 1984. **85**(9): p. 13-15.

35. Renner, G., *Troubleshooting the Yankee Dryer.* Tappi J., 1989. **72**(6): p. 119-122.

36. Atkins, J., J. Luce, and D. Vickery, *Infrared thermography -- aid to solving paper machine moisture profile problems.* Tappi J., 1978. **61**(12): p. 17-20.

37. Korach, C., D. Orloff, and T. Patterson. *High-speed infrared detection of coated-roll surface defects*. in *Engineering and papermakers: forming bonds for better papermaking*. 1997.

38. Lobbes, T. and W. Forester, *The identification of stickies*, in *Paper Recycling Challenge - Stickies*, M. Doshi, Editor. 1997. p. 190-192.

39. Martz, W., *Advanced joint and siphon system for optimal heat transfer and temperature profile.* Corrugating Inernational, 2000. **2**(3): p. 57-59.

40. Murakami, K. and T. Yamaychi, *Observation of deforming process of a poorly formed paper sheet by thermography.* J. of the Society of Fiber Science and Technology, 1994. **50**(9): p. 424-425.

41. Kiiskinen, H., H. Kukkonen, A. Laine, and P. Pakarinen, *Infrared thermography examination of paper structure.* Tappi J., 1997. **80**(4): p. 159-162.

42. Saylor, J., G. Smith, and K. Flack, *The effect of a surfactant monolayer on the temperature field of a water surface undergoing evaporation.* International Journal of Heat and Mass Transfer, 2000. **43**: p. 3073-3086.

43. Flack, K., J. Saylor, and G. Smith, *Near-surface turbulence for evaporative convection at an air/water interface.* Physics of Fluids, 2001. **13**(11): p. 3338-33345.

44. Saylor, J., K. Flack, M. Schultz, and G. Smith, *The correlation between surface temperature and subsurface velocity during evaporative convection.* Experiments in Fluids, 2002. **32**: p. 570-579.

45. Saylor, J., G. Smith, and K. Flack, *Infrared imaging of the surface temperature field of water during film spreading.* Physics of Fluids, 2000. **12**(3): p. 597-602.

46. Dussaud, A., S. Troian, and S. Harris, *Fluorescence visualization of a convective instability which modulates the spreading of volatile surface films.* Physics of Fluids, 1998. **10**(7): p. 1588-1596.

47. Dussaud, A. and S. Troian, *Dynamics of spontaneous spreading with evaporation on a deep fluid layer.* Physics of Fluids, 1997. **10**(1): p. 23-37.

48. Saylor, J., *Determining liquid substrate cleanlines using infrared imaging.* Review of Scientific Instruments, 2001. **72**(12): p. 4408-4414.

49. Phongikaroon, S., K. Judd, G. Smith, and R. Handler, *The thermal structure of a wind-driven Reynolds ridge.* Experiments in Fluids, 2004. **37**: p. 153-158.

50. Fike, G., J. Abedi, and S. Banerjee, *Imaging the Drying of Surfaces by Infrared Thermography.* Ind. Eng. Chem. Res., 2004. **43**: p. 4178-4181.

51. Incropera, F. and D. DeWitt, *Fundamentals of heat and mass transfer*. 4th ed. 1996, New York: Wiley.

52. *ThermaCAM Researcher 2000 Operating Manual*. 2000, FLIR Systems.

53. Bierman, C., *Handbook of Pulping and Papermaking*. 2nd ed. 1996, San Diego, CA: Academic Press.

54. Banerjee, S., W. Su, L. Otwell, M. Hittmeier, and K. Nichols, *Wet line extension reduces VOCs from softwood drying.* Environ. Sci. Technology, 1998. **32**: p. 1303-1307.

55. Su, W., H. Yan, S. Banerjee, L. Otwell, and M. Hittmeier, *Field-proven strategies for reducing VOCs from hardwood drying.* Environ. Sci. Technology, 1999. **33**: p. 1056-1059.

56. Christiansen, A., *How overdrying wood reduces its bonding to phenol-formaldehyde adhesives: a critical review of the literature. Part I. Physical responses.* Wood Fiber Science, 1990. **22**(4): p. 441-459.

57. Christiansen, A., *How overdrying wood reduces its bonding to phenol-formaldehyde adhesives: a critical review of the literature. Part II. Chemical reactions.* Wood Fiber Science, 1991. **23**(1): p. 69-84.

58. Creton, C. and L. Leibler, *How does tack depend on time of contact and contact pressure?* J. Polymer Science B, 1996. **34**: p. 545-554.

59. Creton, C. and P. Fabre, *Tack*, in *to appear in: Comprehensive Adhesion Science, Vol. II, The Mechanics of Adhesion, Rheology of Adhesives, and Strength of Adhesive Bonds*. 2001.

60. Chiche, A., P. Pareige, and C. Creton, *Role of surface roughness in controlling the adhesion of a soft adhesive on a hard surface.* C.R. Acad. Sci. Paris, 2000. **IV**(1): p. 1197-1204.

61. Ahrens, F., B. Hojjatie, and D. Coffin. *Influence of Drying Variables in Development of Cockle: An Experimental Study*. in *International Paper Physics Conference*. 2003. Victoria, British Columbia, Canada: TAPPI & PAPTEC.